Top pair invariant mass distribution: a window on new physics

# Top pair invariant mass distribution: a window on new physics

**Rikkert Frederix and Fabio Maltoni**

*Centre for Particle Physics and Phenomenology (CP3),*
*Université Catholique de Louvain,*
*Chemin du Cyclotron 2, B-1348 Louvain-la-Neuve, Belgium*
*E-mail:* Rikkert.Frederix@uclouvain.be, Fabio.Maltoni@uclouvain.be

ABSTRACT: We explore in detail the physics potential of a measurement of the $t\bar{t}$ invariant mass distribution. First, we assess the accuracy of the best available predictions for this observable and find that in the low invariant mass region, the shape is very well predicted and could be used to perform a top mass measurement. Second, we study the effects of a heavy $s$-channel resonance on the $t\bar{t}$ invariant mass distribution in a model independent way. We provide the necessary Monte Carlo tools to perform the search and outline a simple three-step analysis.

JHEP01(2009)047

# Contents

## 1. Introduction

The top quark is unique among the so-far-discovered matter constituents: it is the only fermion whose mass is very close to the scale of electroweak symmetry breaking (EWSB), $m_t \simeq v/\sqrt{2}$, and therefore it has a naturally strong coupling, $\lambda_t \simeq 1$, to the Higgs boson in the standard model.[1] It is because of this large coupling, for instance, that the Higgs mass can be predicted via precision measurements, and the Higgs can be copiously produced at hadron colliders operating at the TeV scale, via its top-loop mediated interactions to gluons. Thanks to its large mass, the top quark has also been exploited in many scenarios that go beyond the standard model (BSM). The simplest one is SUSY, where top has the important role of triggering EWSB and the historical merit of having escorted the MSSM to the LHC era by allowing the Higgs mass to survive to the LEP bounds.

---

[1]Another numerical coincidence is also often mentioned, namely $m_t \simeq m_W + m_Z$, with somewhat less inspirational effects.

Top has also been the source of inspiration for many alternative mechanisms of EWSB, where it has a direct or indirect role in the boson as well as fermion mass generation: Topcolor [1–4], top see-saw [5–7] and other refinements [8]. More recently, in other theoretical constructions that aim at the stabilization of the Higgs mass, the presence of the top quark requires a mechanism that compensates for its large (negative) radiative corrections to the Higgs mass. In general such mechanisms entail the existence of new particles, *i.e.*, top partners, that can be scalars, like in SUSY, as well as fermions, like in the Little Higgs [9–16] or models with extra dimensions [17, 18]. In addition, in many such models gauge interactions exist whose coupling with the third generation quarks and in particular to the top quark are enhanced. These include Kaluza-Klein (KK) excitations of the graviton [19–21] as well as the weak [22] and the strong gauge bosons [19, 23–30] which couple to top quarks. Such particles could show up as resonances in the $pp \to X \to t\bar{t}$ production channel and not in other channels, like di-jets or di-leptons, due to their small couplings to light particles.

If on the one hand, the fact that many rich and theoretically motivated models predict new physics in connection with the top quark provides a strong motivation for detailed experimental investigations, on the other it makes difficult to perform the analyses corresponding to all the suggested scenarios. A way to avoid such an "explosion" of models is a bottom-up approach, where first a physical observable, which carries some potential for BSM studies, is identified and then the effects due to the existence of new physics are systematically explored. The aim of this paper is to present such a model independent approach to the discovery and identification of new physics in $m_{t\bar{t}}$, the top-antitop invariant mass distribution. We do not focus on specific models, instead we assume the existence of heavy particles, whose masses and quantum numbers are unknown but are such that interactions with the top quark are privileged, a feature common to many scenarios where the top quark plays a role in the EWSB, as discussed above. To simulate the physics associated with the new states, we have developed a dedicated "model" in the multipurpose Monte Carlo generator MadGraph/MadEvent [31–33].[2]

The strategies and the difficulties associated to the accuracy which will be needed for the reconstruction of $m_{t\bar{t}}$ have been the subject of several investigations [34, 35] and are left to dedicated experimental studies. However, we briefly comment on them in appendix A.

The paper is organized as follows. In section 2, we perform an analysis of the theoretical uncertainties on the QCD predictions for $m_{t\bar{t}}$, in the low- as well as high-mass regions. We find that the shape of the $m_{t\bar{t}}$ distribution has very little theoretical uncertainties (in contrast to its normalization, i.e., the total cross section) and we argue it could provide a new handle on the top mass determination.

In sections 3, 4 and 5 we explore a three-step analysis. In section 3 the effects on $m_{t\bar{t}}$ induced by new heavy resonances in the s-channel, $pp \to X \to t\bar{t}$, from the presence of simple peaks, to non-trivial patterns arising from interference between signal and SM background. In the following section we assume that a resonance is found and study how the

---

[2]The Monte Carlo and a wide collection of parton-level data samples (Les Houches format) suitable for further experimental analysis on the scenarios presented in this work, are available on the MadGraph servers, e.g., http://madgraph.phys.ucl.ac.be.
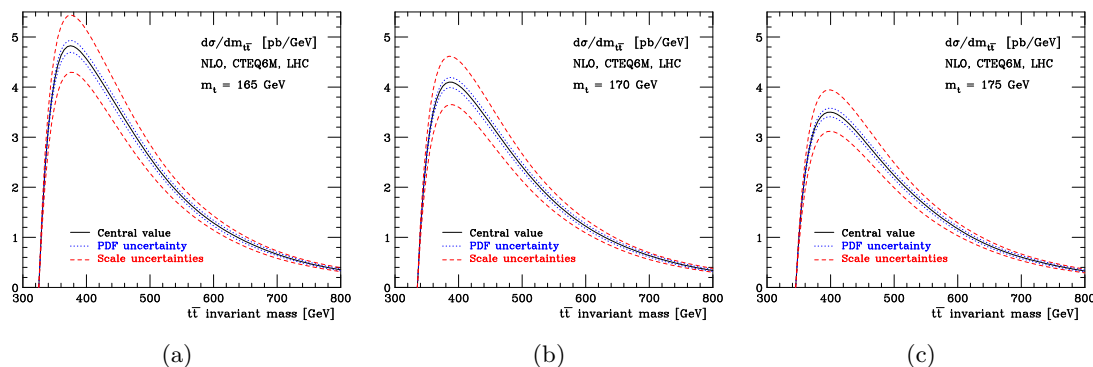
**Figure 1:** Scale (*dashed*) and PDF (*dotted*) uncertainties in the $t\bar{t}$ invariant mass spectrum for top masses (a) $m_t = 165\,\text{GeV}$, (b) $m_t = 170\,\text{GeV}$ and (c) $m_t = 175\,\text{GeV}$ at NLO for the LHC using the CTEQ6M pdf set.

spin structure of a resonance affects the angular distributions of the top and anti-top quarks. In section 5 we discuss how spin-correlations are affected by nature of the coupling of the resonances to SM particles, by simulating the full matrix elements including the decay, $pp \to X \to t\bar{t} \to 6f$. We leave to section 6 the discussion of the results and our conclusions.

## 2. SM theoretical predictions at NLO

In this section we study the theoretical uncertainties on the available predictions for the invariant mass spectrum and their dependence on the top mass. We mainly focus on the LHC and refer to the results of ref. [36] for the Tevatron. We start by considering the invariant mass spectrum of the $t\bar{t}$ pair calculated up to next-to-leading order (NLO), as implemented in MCFM [37]. We use the CTEQ6M PDF-set [38] and do not apply cuts on the final state particles. Here and in the following we always assume that the invariant mass can be fully reconstructed, see also the appendix. In figure 1 results at the LHC are plotted for three different top quark masses with uncertainty bands associated to the PDF errors and renormalization and factorization scale variations.

The PDF uncertainty is estimated by running the 41 members of CTEQ6 PDF set, with the scales set equal to $\mu_R = \mu_F = m_t$, and found to be about $\pm 3.2\%$. The scale uncertainty is obtained by varying independently the renormalization and factorization scales in the region between $\mu_R = \mu_F = m_t/2$ and $\mu_R = \mu_F = 2m_t$. The associated total scale uncertainty at NLO is about $\pm 13\%$. Thus, the theoretical errors at the LHC are completely dominated by the scale uncertainty. This is contrast to the Tevatron where scale and PDF errors are comparable, of the order 6% [36].

NLL resummed calculations suggest that the dependence on the scales could go down to $\pm 6\%$ [39, 40], however in that analysis the scales were not varied independently. A more recent study suggests that changing the scales independently might increase the error to a size similar to that estimated through the NLO fixed order calculation [41].

Next we compare the NLO shapes for the invariant mass distribution with those obtained at LO and MC@NLO [42], figure 2, both at the Tevatron and the LHC. We find
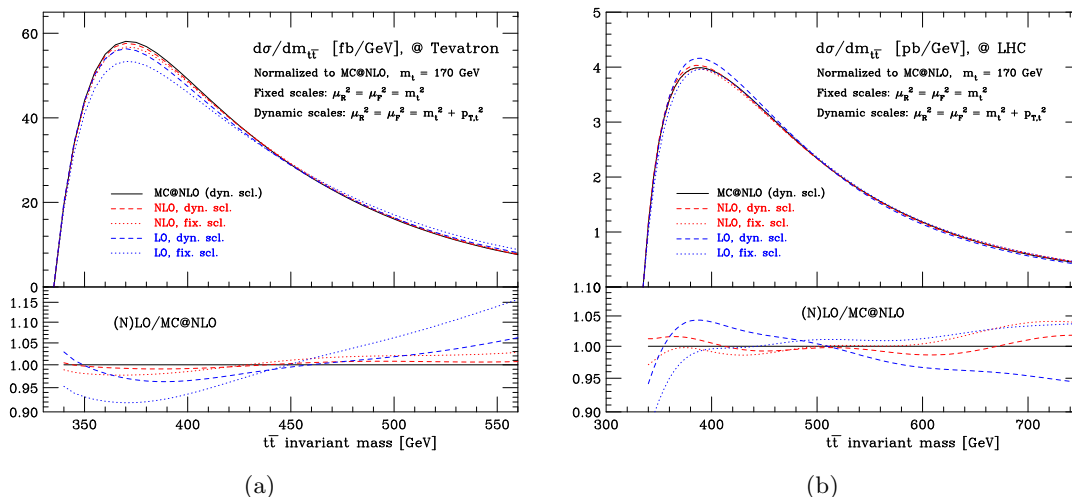
**Figure 2:** The MC@NLO $m_{t\bar{t}}$ distribution compared with the LO (*blue*) and NLO (*red*) fixed order predictions. The distributions are normalized to the MC@NLO cross section. We set $m_t = 170\,\text{GeV}$, include no cuts, and use CTEQ6M for the NLO and MC@NLO, and CTEQ6L1 for the LO calculations.

that the differences are minimal at the LHC, and well within the uncertainty bands of the theoretical errors on the NLO cross section. On the other hand, at the Tevatron the differences between LO and NLO, fixed and dynamic renormalization and factorization scales are larger.

In the high invariant mass region for the LHC, figure 3, the LO approximation starts to deviate from the NLO order and clearly underestimates the NLO distribution (note that curves here are normalized to the total cross section at NLO). Also, as expected, the PDF uncertainties start to increase and dominate the theoretical errors as the most important contributions come from the large $x$ region. Next-to-leading order electroweak corrections to the LO distribution are also included in this figure [43, 44]. Their effect is to decrease the cross section by a few percent for invariant masses below $1000\,\text{GeV}$ and up to 15% for invariant masses around $4\,\text{TeV}$ (the Higgs mass dependence is mild). This means that EW effects on this distribution are negligible compared to the current PDF uncertainties and give only a minor deviation from the LO curve.

We conclude this section by mentioning the other sources of potentially large uncertainties in the determination of the $t\bar{t}$ invariant mass. The first is related to its reconstruction from the decay products. In general the uncertainty on the $m_{t\bar{t}}$ distribution will depend on the final state signature (fully-hadronic, single-lepton and double-lepton final states), which determine the reconstruction technique and, more importantly, on the detector efficiencies and resolutions. For completeness we briefly discuss the current proposals for reconstruction in the various decay channels in the appendix. The second is due to both QCD backgrounds, i.e. multi-jet, $W, Z$+jets and $WW$+jets, and top backgrounds, i.e. single-top and $t\bar{t}$ itself as coming from a final state different signature than the one considered. While the QCD backgrounds at the Tevatron are severe but very well studied, it has been shown that at the LHC their impact at low $t\bar{t}$ invariant mass is negligible when at least one lepton
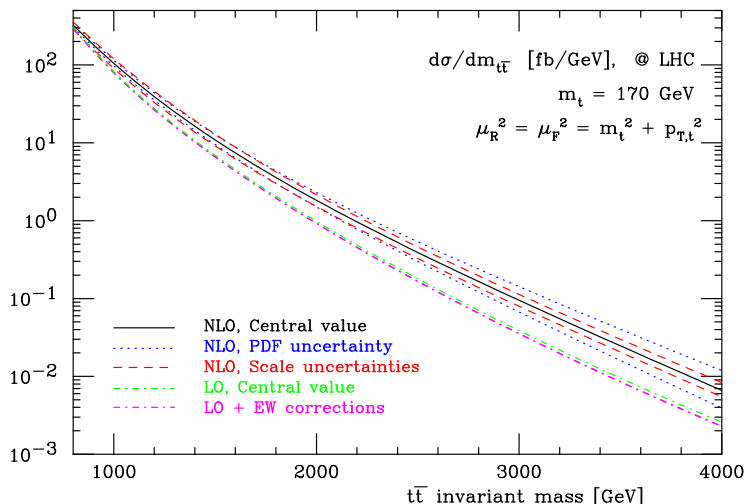
**Figure 3:** Scale (*dashed*) and PDF (*dotted*) uncertainties in the $t\bar{t}$ invariant mass spectrum for $m_t = 170\,\mathrm{GeV}$ at NLO in QCD, with the CTEQ6M PDF-sets. Also plotted are the LO distribution (*light dash-dotted*), the LO including NLO Electro-Weak corrections (*dark dash-dotted*) with CTEQ6L1 PDF-set. The LO distribution is normalized to the NLO total cross section.

is present in the final state [45]. In the high invariant mass tail, some QCD backgrounds, and in particular $W+$ one or two jets, become important due to the fact that the tops are highly boosted and can give rise to single jet-like topologies when they decay hadronically. The interested reader can find a detailed study for the single lepton final state signature in refs. [35, 46].

## 2.1 Top quark mass dependence

As can be clearly seen from figure 1, the normalization, as well as the shape of the $t\bar{t}$ invariant mass distribution depends on the mass of the top quark. It is then natural to wonder whether such a rather strong dependence could provide another way to determine the mass of the top quark. The aim of this subsection is to provide a quantitative answer, based only on the theoretical uncertainties.

In figure 4 we have plotted the $t\bar{t}$ production cross section $\sigma$ as a function of the top quark mass at the Tevatron (a) and the LHC (b). The scale uncertainties, even at the NLO, are rather large. Neglecting non-linear terms, a fit to the central curve gives

$$\Delta m_t/m_t \sim 0.2\Delta\sigma/\sigma + 0.03 \qquad \text{(LHC)}. \tag{2.1}$$

This equation relates the relative uncertainty on the measurement of the $t\bar{t}$ cross section to the relative uncertainty on the top quark mass: the $\Delta\sigma/\sigma$ term represents the slope and the constant term the horizontal spread, i.e., the scale uncertainty, of the curves in figure 4. This means that a measurement of the cross section with an uncertainty of 5% would lead to a $0.2 \times 5\% + 0.03 = 4\%$ uncertainty of the top quark mass, the error being mainly associated with scale variations. At the Tevatron the situation is slightly different.
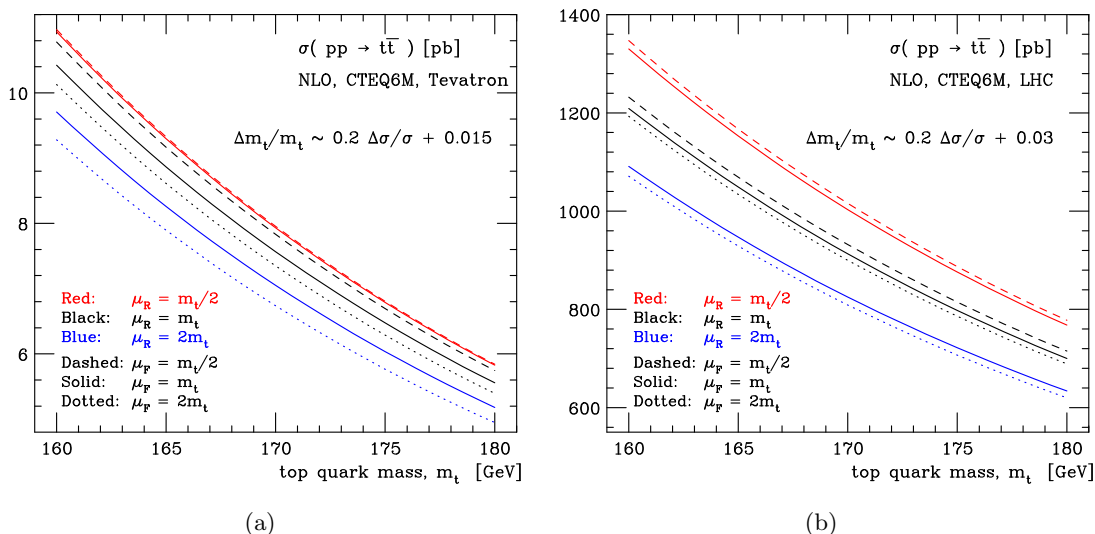
**Figure 4:** The $t\bar{t}$ production cross section as a function of the top quark mass $m_t$ including scale dependence at the Tevatron (a) and the LHC (b).
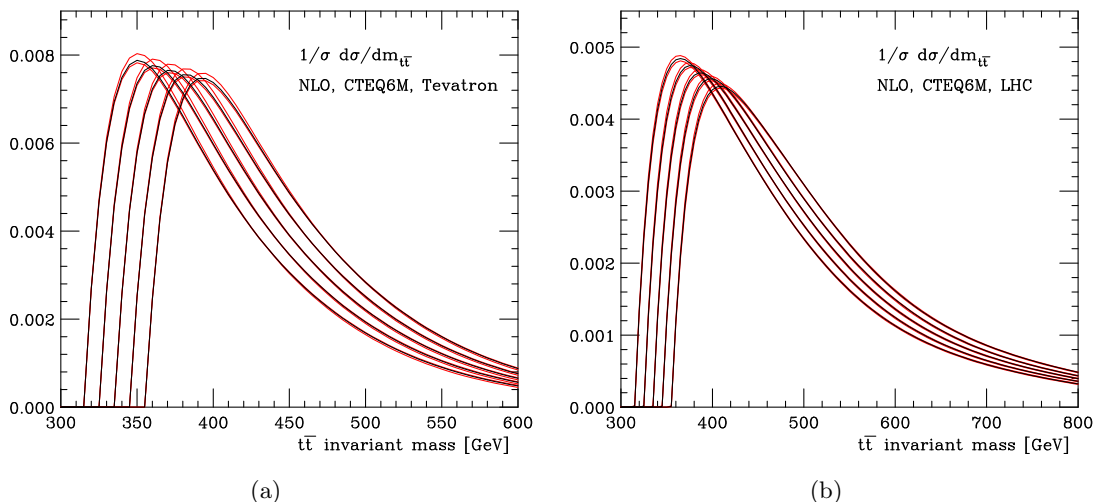


**Figure 5:** The normalized $t\bar{t}$ production cross section as a function of the $t\bar{t}$ invariant mass, $m_{t\bar{t}}$, for the Tevatron (a) and the LHC (b). Solid lines from left to right are for a top quark mass of $m_t = 160, \ldots, 180\,\text{GeV}$ in steps of $5\,\text{GeV}$, respectively. The bands spanned by the red lines show the scale uncertainties.

The scale dependence is milder,

$$\Delta m_t/m_t \sim 0.2 \Delta\sigma/\sigma + 0.015 \qquad (\text{Tevatron})\,, \tag{2.2}$$

and known to be reduced at NLL [36], but the PDF errors, which are not included in the plot, are not negligible and are found to be of a similar size [36].

We can therefore conclude that the accuracy of an independent extraction of the top mass from a measurement of the cross section is limited by the NLO theoretical uncertainties. Recent work suggests that inclusion of NNLO corrections could reduce the scale

uncertainties sizably [47].

It is worth investigating whether information on the top mass can be extracted from some other quantity besides the total cross section. In figure 5 the $t\bar{t}$ invariant mass distributions normalized to unity, $\frac{\partial\sigma}{\partial m_{t\bar{t}}}\big|_{\text{norm.}}$, are plotted for five different top quark masses, $m_t = 160\ldots 180\,\text{GeV}$ in steps of $5\,\text{GeV}$. The bands spanned by the red lines show the left-over scale uncertainties which are sizably reduced compared to figure 1. We find that the shape of the $m_{t\bar{t}}$ distribution is quite insensitive to theoretical uncertainties, while retaining a strong dependence on the top quark mass. It is therefore interesting to consider whether the invariant mass distribution could provide an independent measurement of the top quark mass.

One way to quantify to which extent the shape is sensitive to the top mass vs. the theoretical uncertainties is to perform an analysis based on the first few moments of the normalized $t\bar{t}$ invariant mass distributions $\frac{\partial\sigma}{\partial m_{t\bar{t}}}\big|_{\text{norm.}}$. This approach has the virtue of being simple and systematic. Needless to say, alternative quantities, such as the peak position, or more sophisticated techniques, such as Kolmogorov tests, could also be employed.

In figure 6 we present the mean value $\langle m_{t\bar{t}}\rangle$, standard deviation $s$, skewness $\gamma_1$ and kurtosis $\gamma_2$ of the $t\bar{t}$ invariant mass distributions as a function of the top quark mass $m_t$ for various scales at the LHC. We remind that the skewness (kurtosis) is a dimensionless quantity that gives a measure of asymmetry (peakedness) of a distribution. These quantities are defined as

$$\langle m_{t\bar{t}}\rangle = \int^{m_{\text{cutoff}}} \mathrm{d}m_{t\bar{t}}\, m_{t\bar{t}} \frac{\partial\sigma}{\partial m_{t\bar{t}}}\Big|_{\text{norm.}}, \qquad s = \sqrt{\mu_2}, \qquad \gamma_1 = \frac{\mu_3}{\mu_2^{3/2}} \quad \text{and} \qquad \gamma_2 = \frac{\mu_4}{\mu_2^2} - 3, \tag{2.3}$$

respectively. The central moments $\mu_n$ are defined as

$$\mu_n = \int \mathrm{d}m_{t\bar{t}} \left(m_{t\bar{t}} - \langle m_{t\bar{t}}\rangle\right)^n \frac{\partial\sigma}{\partial m_{t\bar{t}}}\Big|_{\text{norm.}}. \tag{2.4}$$

In our analysis we focus on the low invariant mass region and therefore we have limited the $m_{t\bar{t}}$ integrals to $m_{t\bar{t}} < m_{\text{cutoff}} = 1\,\text{TeV}$. The aim of this cut is just to mimic an experimental analysis where the precision on the higher moments would be limited by the statistics. Since our purpose is only for illustration we do not consider these effects further. However, we stress that our numerical results do retain a significant dependence on this cutoff.

Due to the small scale uncertainty and the strong linear correlation, the mean of the $t\bar{t}$ invariant mass distribution, $\langle m_{t\bar{t}}\rangle$, figure 6(a), appears to be an excellent estimator of the top quark mass. From the experimental point of view, one can also hope for smaller uncertainties than those associated to the measurement of total cross section. In fact, to measure the mean, many systematics, such as those coming from luminosity or tagging efficiencies, are much less important. A fit to the mean value shows that $\Delta m_t/m_t \sim 1.2\Delta\langle m_{t\bar{t}}\rangle/\langle m_{t\bar{t}}\rangle + 0.003$. So, for instance, if the mean value is measured with a 1% uncertainty, the uncertainty of the top quark mass is only 1.3%, including the scale uncertainties.

The standard deviation, figure 6(b), is almost constant and therefore is not suitable for a top quark mass measurement. In figures 6(c) and 6(d) the skewness and the kurtosis for the $t\bar{t}$ invariant mass are plotted, respectively. Also here, the scale uncertainty
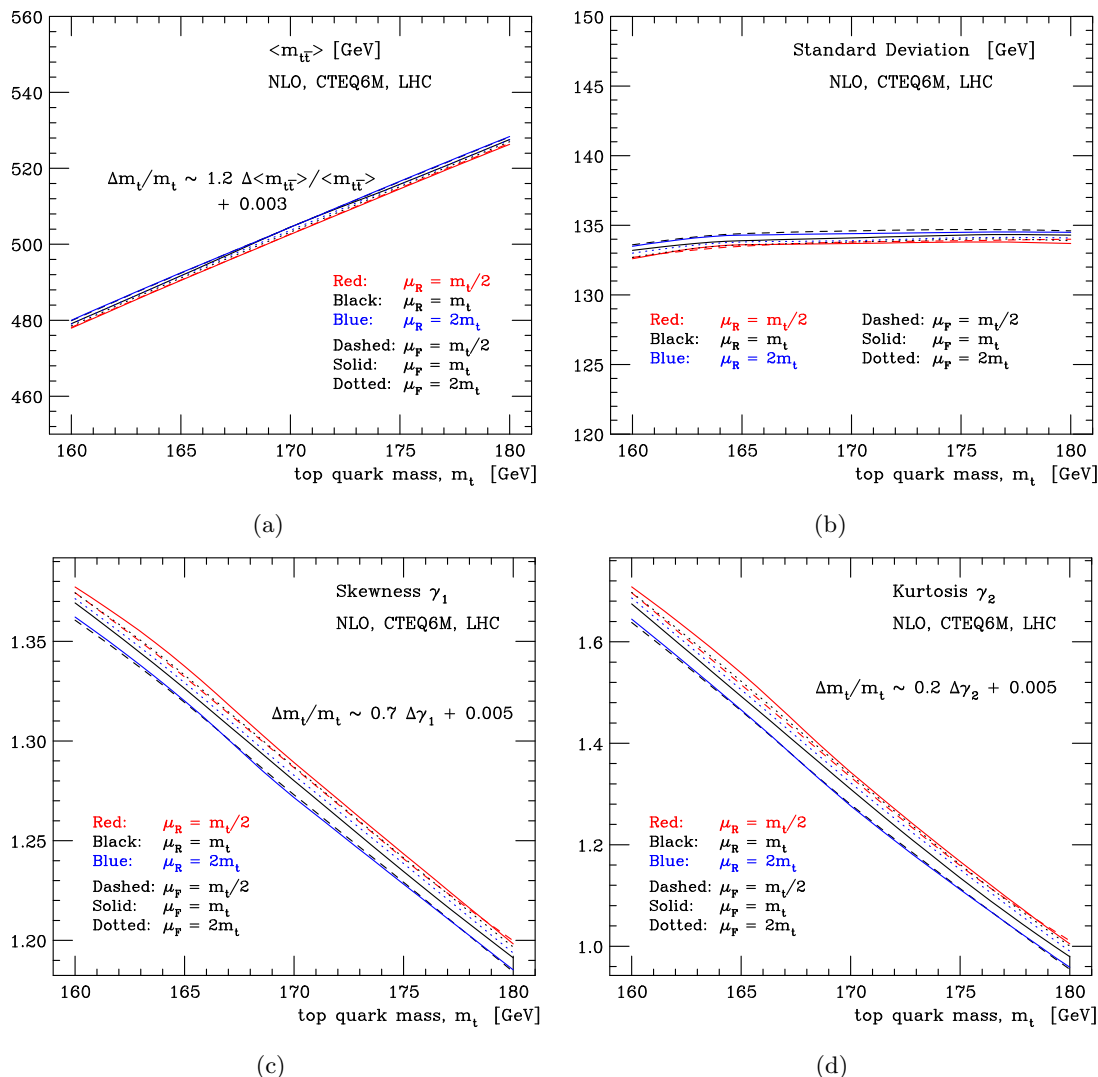
**Figure 6:** The average value (a), standard deviation (b), skewness (c) and kurtosis (d) of the $t\bar{t}$ invariant mass distribution as a function of the top quark mass $m_t$ including the scale dependence at the LHC.

is reduced, while still slightly larger than for the mean value, figure 6(a). The slopes of the lines are promising, in particular for the kurtosis, which means that a relatively large experimental error on the measurement of the kurtosis leads to an only small error on the top mass measurement.

At this point, we have to stress that the above simple analysis does not include neither statistical nor systematics effects in the data, which should also be carefully considered. In particular, the higher moments such as the skewness and the kurtosis are more sensitive to the tail of the $m_{t\bar{t}}$ distribution then the lower moments and therefore more sensitive to statistical and systematic effects that affect more strongly this tail. Eventually, the final uncertainty on the top quark mass will depend on how well the above quantities can be measured. It is plausible to expect that a combined analysis based on the above quantities
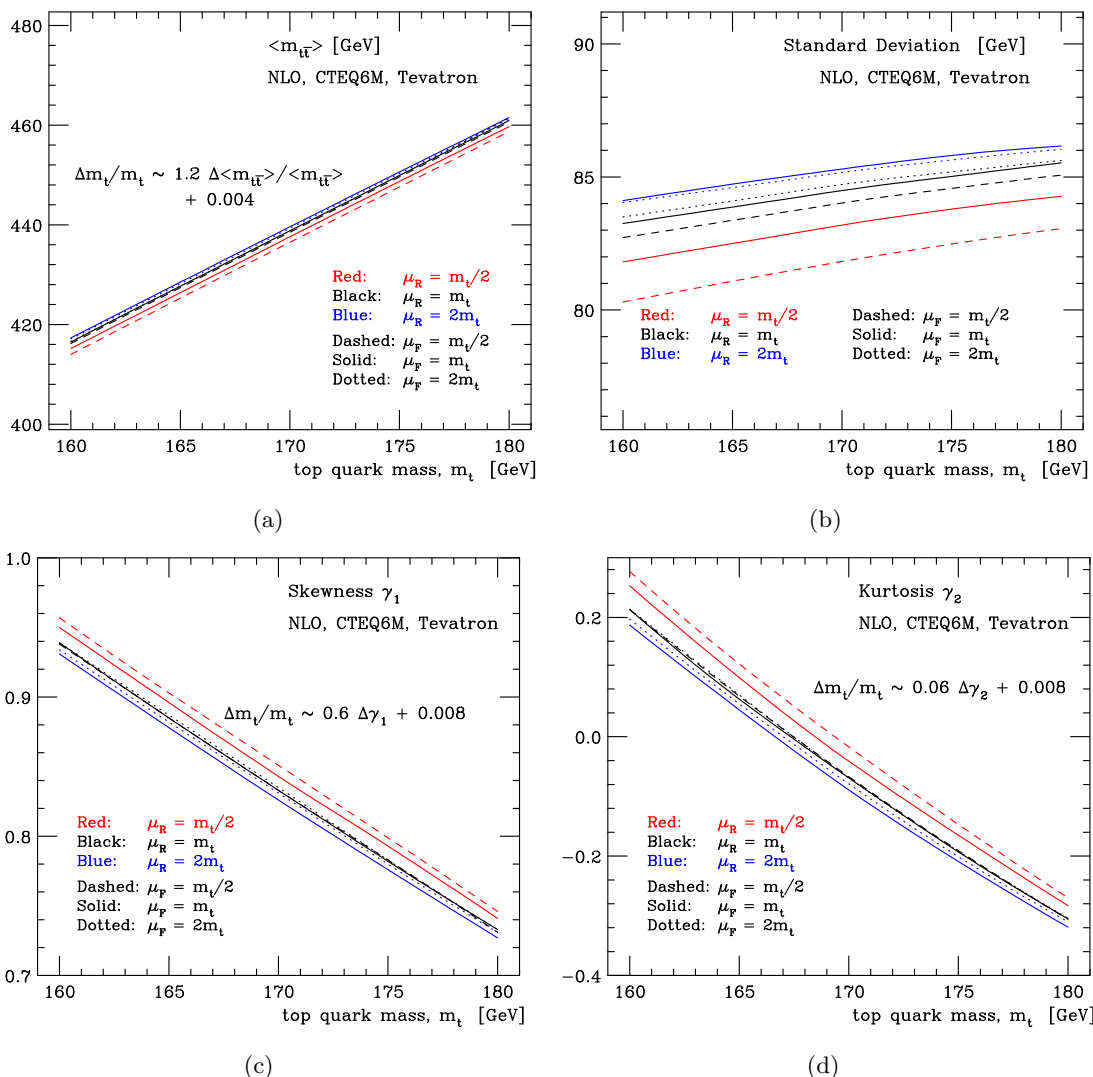
**Figure 7:** The average value (a), standard deviation (b), skewness (c) and kurtosis (d) of the $t\bar{t}$ invariant mass distribution as a function of the top quark mass $m_t$ including the scale dependence at the Tevatron. For the skewness and kurtosis we restricted the integration region in eq. (2.4) to $m_{t\bar{t}} < 600\,\text{GeV}$.

might lead to an even smaller uncertainty for the top quark mass.

For completeness we show the same analysis performed at the Tevatron energies, see figure 7. Also in this case, we have used a fixed order NLO calculation to estimate the scale uncertainties. However, as we have already mentioned, at the Tevatron the $t\bar{t}$ pairs are produced almost at threshold, hence a resummed calculation which predicts a smaller scale uncertainty, is preferred [36].

The Tevatron results (figure 7) are similar to those obtained in the LHC study, but the reduction in the scale uncertainties by analyzing the (higher) moments is smaller compared to the LHC. The first moment, i.e., the mean value, is probably the best estimator for the top quark mass among all the moments, due to its small constant value of 0.004,

and the reasonably good proportionality factor of 1.2. The higher moments are more sensitive to statistical fluctuations and might be less suitable with a limited sample. The lack of events in the higher invariant mass regions might give rise to larger errors for the skewness and worse the kurtosis. In these plots we restrict the $t\bar{t}$ invariant mass to below $m_{\text{cutoff}} = 600\,\text{GeV}$. We mention that even though using the fixed order NLO calculation we have overestimated the scale uncertainties, we have neglected the PDF errors which at the Tevatron can reach the 6-7% [36] and errors coming from the reconstruction of the $t\bar{t}$ invariant mass from the (anti-)top quark decay products, see the appendix.

Finally, we comment about the definition of the top quark mass. As in the more standard top mass measurements where the top mass is reconstructed from its decay products, also the top quark invariant mass is sensitive to extra radiation and to non-perturbative effects due to confinement, typical of a pole mass [48]. In this respect the same issues and problems in associating a theoretically well-defined mass to the measurement remain. This is at variance with an extraction of the top mass from a cross section measurement which can be directly related to a short distance mass and does not suffer from the same non-perturbative or extra radiation effects. We stress, however, that $m_{t\bar{t}}$ is at least twice the top quark mass, which would decrease the relative impact of the ambiguities due to extra radiation. In addition, typical combinatorial systematics associated to the assignment of the jets to the "right" tops, are absent for $m_{t\bar{t}}$. In this respect, more experimental work on the systematics affecting such a measurement would be certainly welcome.

## 3. Effects from BSM resonances

In this section we investigate the effects of (model-independent) new resonances on the $t\bar{t}$ invariant mass spectrum. All the numerical results presented here have been obtained with MadGraph/MadEvent, through the implementation of a dedicated "model", topBSM, which is publicly accessible on the MadGraph servers for on-line event generation and for download.[3]

topBSM offers the possibility of studying a wide range of new physics resonances and efficiently exploits the flexibility and the possibilities of MadGraph:

- SM effects are consistently included, i.e., possibly non-trivial interference effects between new resonances and the $t\bar{t}$ background are taken into account. As it will be shown in the following, in some cases such effects can be important and might lead to very distinctive signatures (cf. the case of the peak-dip structure arising in $m_{t\bar{t}}$ due to the presence of a (pseudo-)scalar state). In general, they should be always included.

- The full matrix elements $2 \rightarrow 6$ including the decays of the top quarks can be generated, which is crucial for spin correlation studies.

- The generated events can be automatically interfaced to parton showers programs, such as Pythia [49] or Herwig [50], to shower and hadronize the events after which these events can be processed by a detector simulation for full experimental analyses.

---

[3]Technical documentation on how to use the model can be found at http://cp3wks05.fynu.ucl.ac.be/twiki/bin/view/Software/TopBSM.

| Spin | color | parity $(1, \gamma_5)$ | some examples/ref. |
|------|-------|------------------------|---------------------|
| 0 | 0 | (1,0) | SM/MSSM/2HDM, ref. [51 – 53] |
| 0 | 0 | (0,1) | MSSM/2HDM, ref. [52, 53] |
| 0 | 8 | (1,0) | ref. [54, 55] |
| 0 | 8 | (0,1) | ref. [54, 55] |
| 1 | 0 | (SM,SM) | $Z'$ |
| 1 | 0 | (1,0) | vector |
| 1 | 0 | (0,1) | axial vector |
| 1 | 0 | (1,1) | vector-left |
| 1 | 0 | (1,-1) | vector-right |
| 1 | 8 | (1,0) | coloron/KK gluon, ref. [56 – 58] |
| 1 | 8 | (0,1) | axigluon, ref. [57] |
| 2 | 0 | — | graviton "continuum", ref. [17] |
| 2 | 0 | — | graviton resonances, ref. [18] |

**Table 1:** The BSM particles included in the `topBSM` "model".

We have considered $s$-channel spin-0, spin-1 and spin-2 resonances, of different color and $CP$ parity, as listed in table 1. The parameters related to each resonance are simply the mass, the width and the relevant values of the couplings to standard model particles which enter in the production process (to the partons and to the top quark).

### 3.1 Spin-0 resonances

The first resonances we discuss are spin-0 particles. We distinguish between color singlet ($\phi$) and color octet ($S^0$), as well as parity even (scalar) and odd (pseudo-scalar) spin-0 particles.

#### 3.1.1 Color singlet

Let us start by considering a color singlet (pseudo-)scalar boson $\phi$ contributing to the $t\bar{t}$ process $gg \rightarrow (\phi \rightarrow)t\bar{t}$. The Feynman diagram for this loop induced process is depicted in figure 8. The spin-0 coupling strength to quarks,

$$g_{\phi qq} = a_1 i \frac{m_q}{v} + a_2 \frac{m_q}{v} \gamma_5, \tag{3.1}$$

is proportional to the quark mass $m_q$. In analogy with the SM, $v$ is the spin-0 field vacuum expectation value and $a_1$ and $a_2$ are real proportionality factors for the parity even and odd spin-0 particles, respectively. For the SM Higgs boson $a_1 = 1$ and $a_2 = 0$, while for a pure pseudo-scalar $a_1 = 0$ and $a_2$ is non-zero.

We do not include scalar production by (anti-)quark annihilation, $q\bar{q} \rightarrow \phi$, because for this cross section to be sizeable compared to the loop induced gluon fusion process, the branching ratio for the scalar to $t\bar{t}$ has to be small and can be neglected.

Since we are interested in scalars with strong couplings to the top quark, we neglect all particles in the loop of figure 8 except for the most heavy quark, i.e., the top quark. If the mass of the spin-0 boson is larger than twice the mass of the top quark, the loop-induced
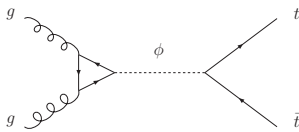
**Figure 8:** Feynman diagram for the (pseudo-)scalar contribution to $t\bar{t}$ production.

gluon-gluon-(pseudo-)scalar coupling develops an imaginary part, which leads to a peak-dip structure for the interference terms between the QCD background and the signal [51 – 53].

The possibility to detect a signal in the $t\bar{t}$ invariant mass depends on the width of the spin-0 resonance. In general, a scalar particle couples also to the electroweak bosons. In the SM the decay rate to $W, Z$ is much larger than the decay rate to $t\bar{t}$, and therefore the $t\bar{t}$ channel is suppressed. Moreover, the presence of a destructive interference between the signal and the QCD background and the relatively large width of the scalar makes detection very difficult. An enhanced coupling to top would not help much because the improvement in the branching ratio would be compensated by an increase of the total width. In conclusion, there is little hope to see a SM-like scalar by looking at the $t\bar{t}$ invariant mass spectrum, even if the coupling to top quark were (much) larger than in the SM.

On the other hand, the case of a pseudo-scalar or a 'boson-phobic' scalar resonance that does not couple to the heavy vector bosons is more promising. For such a state, the branching ratio to $t\bar{t}$ can be taken unity, $\mathrm{BR}(\phi \to t\bar{t}) = 1$, i.e., the total width of the scalar spin-0 resonance is equal to the SM partial width to $t\bar{t}$. SUSY models with this feature can be constructed [59]. The smaller widths of the pseudo-scalar and the boson-phobic scalar give a narrow resonance peak in the $t\bar{t}$ invariant mass spectrum. The interference between the signal and the QCD $t\bar{t}$ production leads to a dip in $t\bar{t}$ production at an invariant mass just above the mass of the spin-0 particle. In this case the signal together with the interference terms sum to the characteristic peak-dip structure, figure 9.

The *dot-dashed* line in figure 9 shows the effect of a $400\,\mathrm{GeV}$ color singlet spin-0 particle on the $t\bar{t}$ invariant mass spectrum with couplings $a_1 = 1$, $a_2 = 0$ and $a_1 = 0$, $a_2 = 1$ for the *left* and the *right* plots, respectively. Comparing with the QCD $t\bar{t}$ production, the *dark solid* line, a peak-dip structure is visible when the spin-0 particle is a pseudo-scalar, $a_1 = 0$ and $a_2 = 1$. In the case where it is a scalar, $a_1 = 1$ and $a_2 = 0$, there is only a peak and a very small dip.

If the coupling to the top quark is enhanced, the peak as well as the dip becomes broader due to the larger decay width. The peak increases in the case the spin-0 is a scalar, but remains the same for the pseudo-scalar. The *dashed* line shows the effect of enhancing the $ttH$ coupling by a factor of two. If the coupling to the top quarks is taken even larger, the increasing width of the (pseudo-)scalar starts to dominate the effects on the invariant mass. This results in the disappearance of the dip, as shown by the *light solid* line in figure 9.

In the case where the coupling to the top is smaller than in the SM, the peak of the scalar gets smaller and the dip completely disappears. The effect of varying the coupling
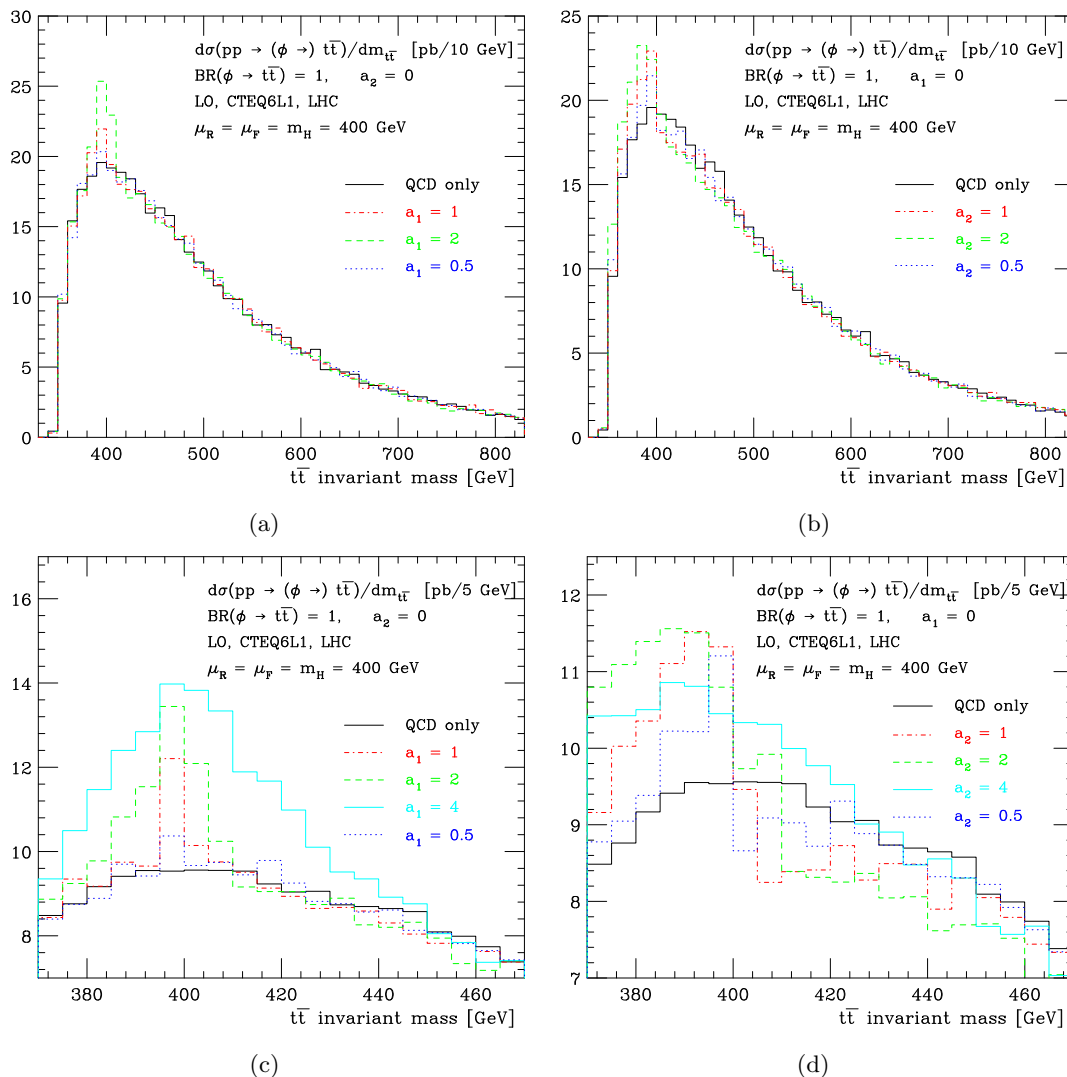
**Figure 9:** Invariant $t\bar{t}$ mass spectrum for the boson-phobic scalar (*left*) and pseudo-scalar (*right*). *Bottom*: The interesting region with finer binning. Different colors represent different coupling strength of the Higgs to top quarks: *dot-dashed* for the standard model coupling and *dotted*, *dashed* and *light solid* for 0.5, 2 and 4 times the standard model coupling strength, respectively. *Dark solid* is QCD $t\bar{t}$ production, i.e., without the Higgs signal. All plots were produced using the CTEQ6L1 pdf set with $\mu_R = \mu_F = 400\,\text{GeV}$. No acceptance cuts are applied.

for the pseudo-scalar are much smaller. Even if the coupling to top quarks is reduced by a factor of two, $a_1 = 0$ and $a_2 = 0.5$, a very clear peak-dip structure is still visible, as shown by the *dotted* line in figure 9.

### 3.1.2 Color octet

The case of a color octet resonance is very similar. Here we shall study scalar $S_R^0$ and a pseudo-scalar $S_I^0$ color octets, similar to those introduced in refs. [54, 55]. In these models the (pseudo-)scalar color octet couples only to quarks, with the same SM coupling but for
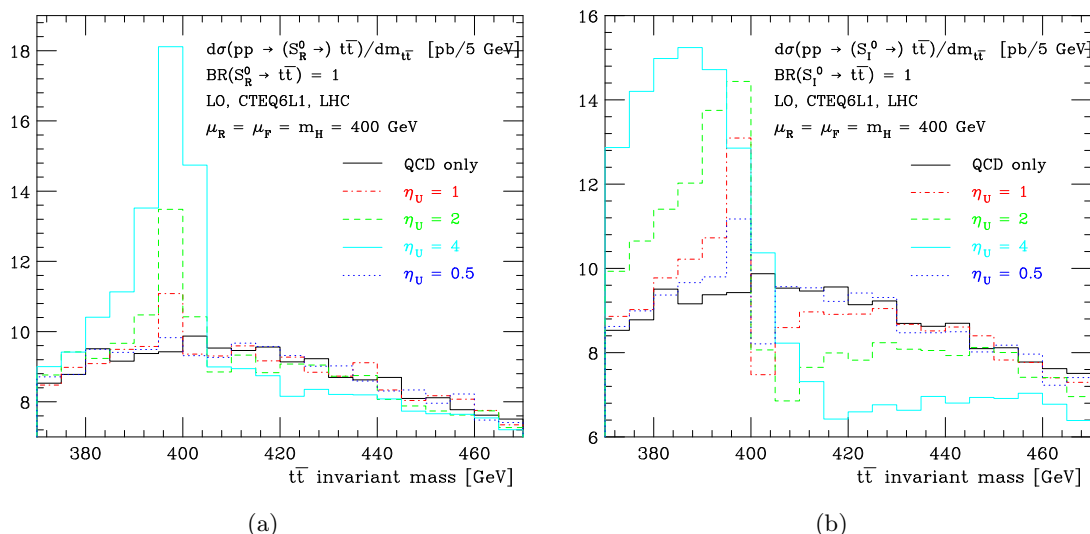
**Figure 10:** Invariant $t\bar{t}$ spectrum for $pp \to t\bar{t}$ including a $s$-channel $S_R^0$ scalar color octet (a) and a pseudo-scalar scalar $S_I^0$ color octet (b) with masses $m_{S_R^0} = m_{S_I^0} = 400\,\text{GeV}$. *Dark solid* line is QCD $t\bar{t}$ production, *dash-dotted* line is with standard coupling between the scalar and $t\bar{t}$, *dashed*, *light solid* and *dotted* the coupling is 2, 4 and 0.5 times as large, respectively. All plots were produced using the CTEQ6L1 pdf set with $\mu_R = \mu_F = 400\,\text{GeV}$. No acceptance cuts are applied.

the color

$$g_{S_R^0 qq} = \eta_U i \frac{m_q}{v} T_{ij}^a, \qquad \text{and} \qquad g_{S_I^0 qq} = \eta_U \gamma_5 \frac{m_q}{v} T_{ij}^a, \qquad (3.2)$$

where $\eta_U$ is a coupling proportionality factor and of order 1. The production and decay mechanism for the (pseudo-)scalar color octet are similar to the 'peak-dip' color singlets, i.e., the resonance is produced through a top quark loop by gluon-gluon fusion, and the decay is mainly to top quarks. We find that compared to the 'peak-dip' color singlet the 'signal' cross section is 5/72 times smaller, i.e., $\sigma(gg \to S_{R,I}^0 \to t\bar{t}) = \frac{5}{72}\sigma(gg \to H \to t\bar{t})$, the interference between signal and background is 5/12 times smaller and the width of the (pseudo-)scalar color octet is 6 times smaller than the width of the 'peak-dip' (pseudo-)scalar color singlet. In figure 10(a) the $t\bar{t}$ invariant mass is plotted in a model with a color octet scalar of a mass of 400 GeV, and in figure 10(b) for the pseudo-scalar. As expected, the results are very similar to the color singlet, see the lower plots of figure 9. The same 'peak-dip' structure is also present for the color octet but it is more pronounced. This is mainly due to the smaller width of the (pseudo-)scalar color octet.

We conclude this section by mentioning that pseudo-scalar singlet and octet resonances could also arise from bound states of meta-stable gluinos in split SUSY scenarios [60]. Also in this case $gg \to \phi$ would be the dominant production channel and it could be described within the same framework.

## 3.2 Spin-1 resonances

In this section we discuss a spin-1 resonance produced by $q\bar{q}$ annihilation. This resonance can either be a color singlet or a color octet. For the color octet case we distinguish
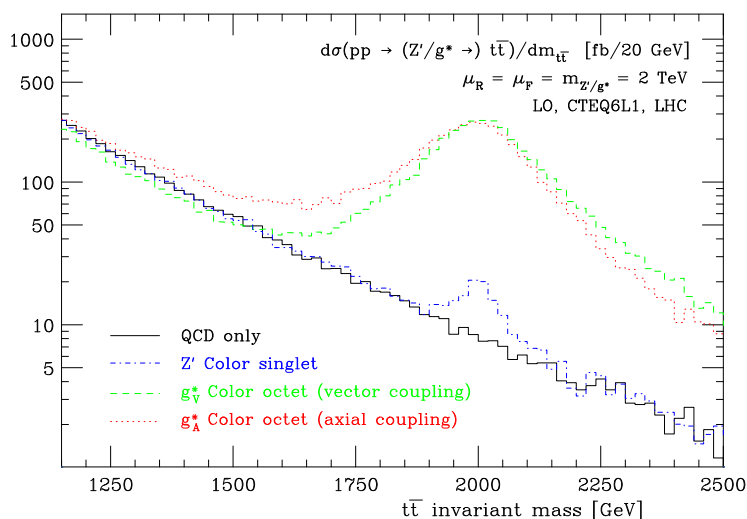
**Figure 11:** Invariant $t\bar{t}$ spectrum for $pp \to t\bar{t}$ including a $s$-channel $Z'$ color singlet vector boson and color octet (axial) vector bosons with masses $m_X = 2000\,\text{GeV}$ that couples with standard model strength to quarks. *Solid* QCD $t\bar{t}$ production, *dotdashed* with a color singlet ($Z'$), *dotted* with a color octet axial vector (axigluon $g_A^*$), *dashed* with a color octet vector boson (KK gluon/coloron $g_V^*$). All plots were produced using the CTEQ6L1 pdf set with $\mu_R = \mu_F = 2000\,\text{GeV}$. No cuts were applied in making any of the plots.

between a vector and an axial-vector. Although both the vector and the axial-vector interfere with the QCD $t\bar{t}$ production, only the vector shows interference effects in the $t\bar{t}$ invariant mass spectrum.

Including an $s$-channel color singlet vector boson (a "model-independent" $Z'$) in the $t\bar{t}$ production process gives a simple peak in the invariant mass spectrum as can be seen from the *dot-dashed* line in figure 11. The precise width and height of the peak depends on the model parameters in the model for the $Z'$. As a benchmark we show a $Z'$ vector boson with mass $m_{Z'} = 2\,\text{TeV}$ that couples with the same strength to fermions as a standard model $Z$ boson. The interference effects with the SM $Z$ boson can be neglected in the $t\bar{t}$ channel, so the peak is independent of the parity of the coupling.

In general, for the color octet spin-1 particles the interference with the SM $t\bar{t}$ production cannot be neglected. Two cases are to be considered: a color octet vector particle (e.g., a KK gluon [58] or coloron [57]), and an axial-vector particle (e.g., an axigluon [61, 62, 57]). It is natural to assume a coupling strength equal to the strong (QCD) coupling $g_s$ for their coupling to quarks.

In figure 11 the effects of a color octet spin-1 particle on the $t\bar{t}$ invariant mass spectrum are presented. The interference effects of the axial vector (*dotted* line) with the QCD $t\bar{t}$ production does not change the shape of the $t\bar{t}$ invariant mass spectrum. Hence the effects of the color octet axial vector and the color singlet are very similar, apart from the size due to the different coupling constant.

The interference of the color octet vector particle with the QCD $t\bar{t}$ production does effect the $t\bar{t}$ invariant mass distribution. There is negative interference in the invariant mass

region below the resonance mass and positive interference for heavier invariant masses. This slightly changes the shape of the peak as can be seen from figure 11. Other quantities, such as the charge asymmetry between the top and the anti-top quarks could be more sensitive to axial vectors [63] and could help their discovery at higher invariant masses.

### 3.3 Spin-2 resonances

The interactions between spin-2 particles, or *gravitons*, and ordinary matter is in general Planck suppressed, which makes it impossible to see effects of the gravitons at TeV energies. There are, however, models with extra dimensions where the contributions from the gravitons might be large enough to make a discovery at the LHC. In this case a model-independent approach is not really appropriate. Instead we consider two scenarios that have distinct signals in the $t\bar{t}$ invariant mass. First the ADD model [17, 64], where the effect of a the large number of graviton KK states contributing to a cross sections could be important and, secondly, the RS model [18, 65] where only a limited number of KK modes contribute, but the coupling constant itself is enhanced by a large "warp" factor.

In the so-called ADD models [17, 64] all SM fields are confined to a four-dimensional brane, letting only gravitons propagate through the bulk. The extra $n$ bulk dimensions are compactified on a $n$-torus with a radius $R$. If the radius $R$ is large enough, (of the order of 0.1 mm for 2 extra dimensions) the $(4 + n)$ dimensional Planck scale can be as small as the TeV scale.

Due to the fact that the radius of the extra dimensions is large, the graviton KK states can be almost degenerate in mass. So, although all graviton couplings are Planck suppressed, the sum of all the KK states can contribute significantly to the $t\bar{t}$ invariant mass spectrum. All states are summed up to the cutoff scale $M_S$, defined by $\lambda^2 R^n = 8\pi(4\pi)^{n/2}\Gamma(n/2)M_S^{-n+2}$, where $\lambda$ is related to the four dimensional Newton's constant $\lambda = \sqrt{16\pi G_N}$.

The effect of this tower of graviton states on the $t\bar{t}$ invariant mass distribution is plotted in figure 12 in the case of 3 extra dimensions and for 4 different cutoff scales. Due to the sum over all nearly degenerate resonances, there is no single resonance peak in the invariant mass distribution. It is also clear that the distribution is only valid well below the cutoff scale $M_S$, otherwise unitarity violating effects become sizable.

In the so-called RS model [18, 65] there is one extra dimension postulated that is compactified to a $\mathbf{S}^1/\mathbf{Z}_2$ orbifold. There are two branes on specific points of the orbifold: a "Planck" brane at $\phi = 0$ and a "TeV" brane at $\phi = \pi$ where the physical SM fields are confined. The bulk space is warped in such a way that the (reduced) Planck mass is warped down on the "TeV" brane to $\Lambda = \overline{M}_{\mathrm{pl}}e^{-\pi\kappa R}$. The gauge hierarchy problem ($\Lambda = \mathcal{O}(1\ \mathrm{TeV})$) is now solved with only a minor fine-tuning of $\kappa R \simeq 12$. After KK compactification of the massless graviton field, the coupling constant of KK gravitons with matter is given by the inverse of $\Lambda$.

A prediction in the RS model is that the masses of the KK modes $m_n$ are given by $m_n^2 = x_n\kappa e^{-\pi\kappa R}$, where $x_n$ are the positive zero's of the Bessel function $J_1(x)$. If one of the masses is given, all the others are fixed, which could give rise to a series of resonances in the $t\bar{t}$ invariant mass spectrum.
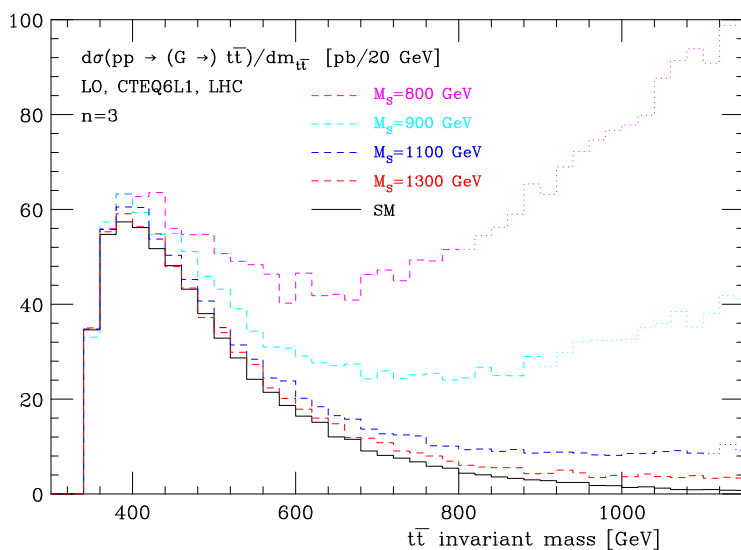
**Figure 12:** Invariant $t\bar{t}$ spectrum for $pp \to t\bar{t}$ including $s$-channel gravitons. The distributions show the effect of the almost degenerate tower of KK gravitons in the ADD model with $n = 3$ extra dimensions and, from top to bottom, with a cutoff scale $M_S = 800, 900, 1100$ and $1300\,\text{GeV}$. The bottom line are contributions from SM only. We used CTEQ6L1 and set the scales to $\mu_R = \mu_F = m_t$.
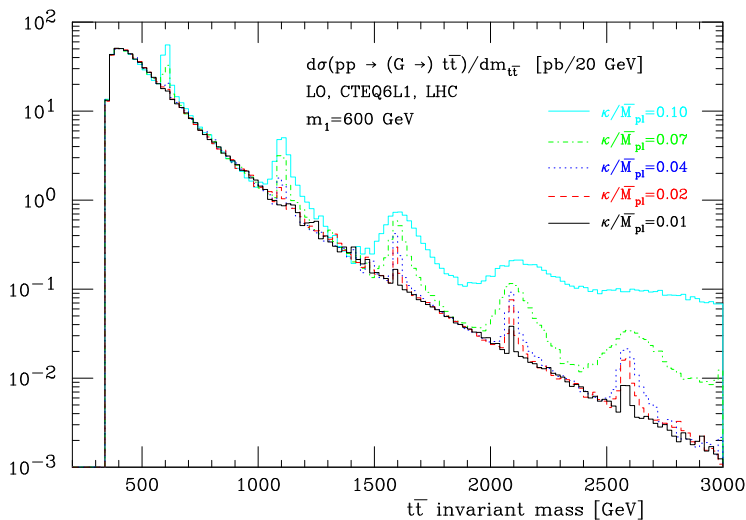


**Figure 13:** Invariant $t\bar{t}$ spectrum for $pp \to t\bar{t}$ including $s$-channel gravitons. The distribution shows the effect of a couple of KK resonances in the RS extra dimensions model. The mass of the first KK mode is $m_1 = 600\,\text{GeV}$ and the colored lines represent various choices for the ratio $\kappa/\overline{M}_{\text{pl}}$. We used CTEQ6L1 and set the scales to $\mu_R = \mu_F = m_t$.

In figure 13 the effect of a series of KK graviton modes on the $t\bar{t}$ invariant mass spectrum is shown with $m_1 = 600\,\text{GeV}$ and for various ratios $\kappa/\overline{M}_{\text{pl}}$. The resonances are clearly visible over the QCD background. Higher KK states are characterized by larger widths.
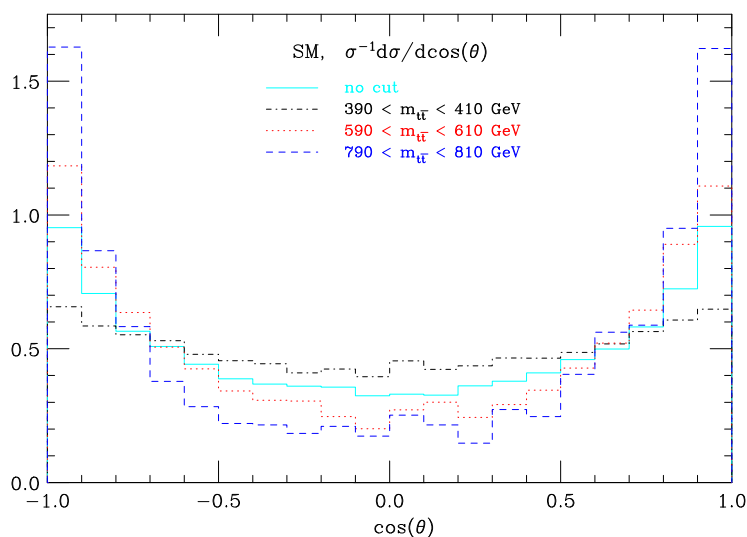
**Figure 14:** Normalized distribution for $\cos\theta$, where $\theta$ is the Collins-Soper angle, for SM production at the LHC. Different lines represent different cuts on $t\bar{t}$ invariant mass.

## 4. Spin information from (anti-)top quark directions

A useful, yet simple, quantity sensitive to the spin of the intermediate heavy state into a $t\bar{t}$ pair, is the Collins-Soper angle $\theta$ [66]. This angle is similar to the angle between the top quark and the beam direction, but minimizes the dependence on initial state radiation. $\theta$ is defined as follows. Let $p_A$ and $p_B$ be the momenta of the incoming hadrons in the rest frame of the top-antitop pair. If the transverse momentum of the top-antitop pair is non-zero, then $p_A$ and $p_B$ are not collinear. The angle $\theta$ is defined to be the angle between the axis that bisects the angle between $p_A$ and $p_B$ and the top quark momentum in the $t\bar{t}$ rest frame.

### 4.1 Standard Model

The distribution of $\theta$ in the SM is plotted in figure 14. Also plotted in the same figure are the distributions with cuts on the $t\bar{t}$ invariant mass spectrum as backgrounds to narrow resonances.

A simple analytic calculation confirms this behavior. The matrix element squared for the initial state $q\bar{q}$ to the SM $t\bar{t}$ contribution in terms of the Collins-Soper angle $\cos\theta$ is proportional to

$$|\mathcal{M}(q\bar{q} \to t\bar{t})|^2 \sim s(1 + \cos^2\theta) + 4m_t^2(1 - \cos^2\theta), \tag{4.1}$$

where $s$ is the center of mass energy squared, $s = (p_q + p_{\bar{q}})^2$. For the $gg$ initial state we have

$$|\mathcal{M}(gg \to t\bar{t})|^2 \sim$$
$$\frac{s(7 + 9\cos^2\theta) - 36m_t^2\cos^2\theta}{\left(sc_- + 4m_t^2\cos^2\theta\right)^2}\left[s^2c_+c_- + 2sm_t^2\Big(3c_-^2 + c_+^2\Big) - 4m_t^4\Big(3c_-^2 + c_+^2 + c_-\Big)\right], \tag{4.2}$$

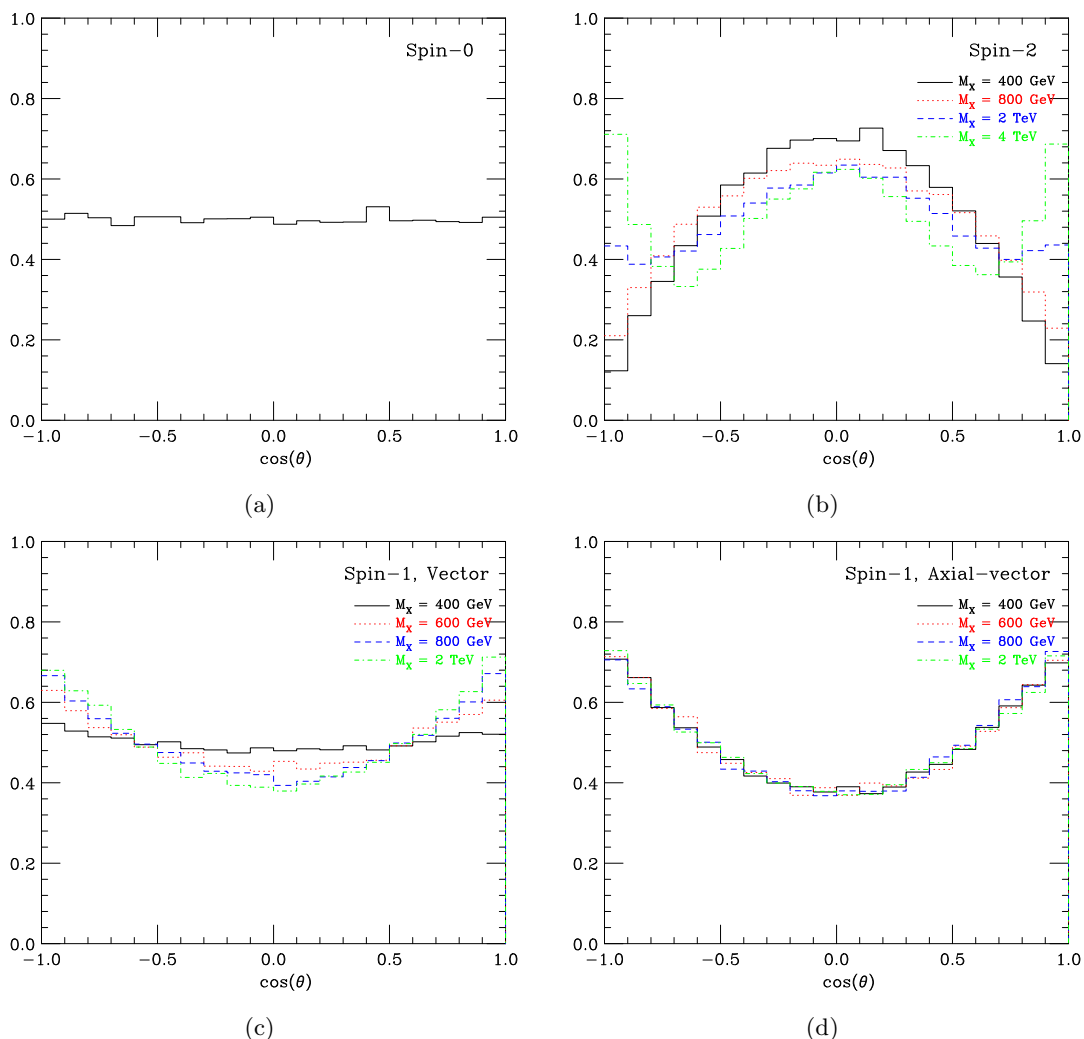where $c_+ = 1 + \cos^2\theta$ and $c_- = 1 - \cos^2\theta$.

**Figure 15:** Normalized distributions for $\cos\theta$, where $\theta$ is the Collins-Soper angle, for spin-0 (a), spin-2 (b), vector (c) and axial-vector (d) resonances of mass $M_X$. All plots were produced using the CTEQ6L1 pdf set with $\mu_R = \mu_F = M_X$.

## 4.2 Spin-0 resonances

In figure 15(a) the normalized cross section as a function of $\cos\theta$ is plotted for a spin-0 resonance. The distribution is independent of the mass and parity of the resonance. The matrix element squared for the spin-0 resonance $H$ is at leading order proportional to

$$|\mathcal{M}(gg/q\bar{q} \to H \to t\bar{t})|^2 \sim (|a_1|^2 + |a_2|^2)p_t \cdot p_{\bar{t}} - (|a_1|^2 - |a_2|^2)m_t^2, \qquad (4.3)$$

where $p_t$ and $p_{\bar{t}}$ are the momenta of the top and anti-top quarks, respectively, and $a_1$ and $a_2$ are the coupling constants, see eq. 3.1, for the scalar and pseudo-scalar, respectively. The matrix element squared is clearly independent of the angle $\cos\theta$, which explains the flat distribution.

### 4.3 Spin-1 resonances

For a generic spin-1 resonance $Z'$ the matrix element squared is proportional to

$$|\mathcal{M}(q\bar{q} \to Z' \to t\bar{t})|^2 \sim 2(|a_L|^4 + |a_R|^4)p_q \cdot p_{\bar{t}} \, p_{\bar{q}} \cdot p_t + 4|a_L|^2|a_R|^2 p_q \cdot p_t \, p_{\bar{q}} \cdot p_{\bar{t}}$$
$$+ m_t^2(|a_L|^2 + |a_R|^2)(a_L a_R^* + a_R a_L^*)p_q \cdot p_{\bar{q}}, \quad (4.4)$$

where $a_L$ and $a_R$ are the left and right handed part of the couplings of the $Z'$ resonance to quarks, i.e., $g_{Z'q\bar{q}} \sim a_L\frac{1-\gamma_5}{2} + a_R\frac{1+\gamma_5}{2}$ and where $p_q$ and $p_{\bar{q}}$ are the momenta of the incoming quark and anti-quark, respectively. In terms of $\cos\theta$ the matrix element squared is proportional to

$$|\mathcal{M}(q\bar{q} \to Z' \to t\bar{t})|^2 \sim (|a_L|^2 + |a_R|^2)(s - 4m_t^2)(1 + \cos^2\theta) + 4m_t^2|a_L + a_R|^2. \quad (4.5)$$

The normalized $\cos\theta$ distribution is independent of the mass of the resonance for a axial vector, $a_R = -a_L$ (see figure 15(d)), while for a pure vector resonance the dependence is maximal figure 15(c). However, for heavy resonances, $M_X \gtrsim 800\,\text{GeV}$ the difference between the curves for the vector and the axial-vector is less then 8% which makes it challenging to get any information about parity of the coupling from this distribution. In ref. [34] a similar polar angle has been studied. That polar angle is also sensitive to the chirality of the coupling. However, the Collins-Soper angle used here has the advantage that it minimizes the effects from initial state radiation.

### 4.4 Spin-2 resonances

In the case of the spin-2 resonance $G_{\mu\nu}$, both the $q\bar{q}$ and $gg$ initial states contribute. The matrix element squared for the $q\bar{q}$ initial state is proportional to

$$|\mathcal{M}(q\bar{q} \to G_{\mu\nu} \to t\bar{t})|^2 \sim s(1 - 3\cos^2\theta + 4\cos^4\theta) + 16m_t^2\cos^2\theta(1 - \cos^2\theta), \quad (4.6)$$

and for the $gg$ initial state

$$|\mathcal{M}(gg \to G_{\mu\nu} \to t\bar{t})|^2 \sim \left[s(1 + \cos^2\theta) + 4m_t^2(1 - \cos^2\theta)\right](1 - \cos^2\theta). \quad (4.7)$$

The large differences in the distributions for the spin-2 resonances between light compared to heavy spin-2 particles, see figure 15(b), is due to the fact that the relatively light spin-2 particles are mainly produced by gluon fusion, while the very heavy spin-2 particles by quark-antiquark annihilation.

## 5. Spin correlations in (anti-)top-quark decays

In the standard model, the semi-weak top-quark decay width is rather large $\Gamma \approx 1.5$ GeV $> \Lambda_{\text{QCD}}$ and top quarks do not form bound hadronic states. At present, we do not have any direct measurement of the top width and the formation of top hadrons is not excluded. This could happen for example, if $V_{tb}$ were much smaller than what is predicted in the standard model, as discussed in ref. [67]. Note, however, that even if this were to happen,

the information on the spin of the top quark would be anyway fully inherited by its decay products [68], as spin-flip would occur at time scales of the order $m_t/\Lambda_{\mathrm{QCD}}^2$, i.e., much later than the lifetime of the top quark. In this respect, spin correlation effects are a very robust probe of new physics entering in the production cross section.

For standard model leptonic top decays, the directions of the leptons are 100% correlated with the polarization of the top quarks. The spin analyzing power of the direction of the $b$ quark ($W^+$ boson) is not as good, around $-0.4$ (0.4). In hadronic top decays the anti-down (or anti-strange) quarks coming from the $W^+$ boson decay have the same full spin analyzing power as the lepton. On the other hand, the up (or charm) quarks have a spin analyzing power of only $-0.3$, i.e., the same as the neutrino in leptonic decays. For the decay of anti-top quarks or spin-down top quarks, all spin analyzing powers change sign. The angular distributions of the two down-type fermions (leptons in leptonic top decays or jets coming from down-type quarks in hadronic $W$ decays) give maximal information about the spin of the (anti-)top quarks in $t\bar{t}$ events [69, 70].

In studies on the spin correlations in $t\bar{t}$ production, two distributions are usually considered [40, 71]. First the distribution

$$\frac{1}{\sigma}\frac{d^2\sigma}{d\cos\theta_+ d\cos\theta_-} = \frac{1}{4}\Big(1 - A\cos\theta_+\cos\theta_- + b_+\cos\theta_+ + b_-\cos\theta_-\Big), \qquad (5.1)$$

where $\theta_+$ ($\theta_-$) is the angle between the $t$ ($\bar{t}$) direction in the $t\bar{t}$ center of momentum frame and the $f_d^+$ ($f_d^-$) direction in the $t$ ($\bar{t}$) rest frame, where $f_d^+$ ($f_d^-$) is the down-type fermion coming from the $W^+$ ($W^-$) decay. For a parity conserving $t\bar{t}$ production mechanism, such as QCD, the parameters $b_+$ and $b_-$ vanish. In practice, the way to construct these angles is first to construct the $t$ and $\bar{t}$ four-momenta in the laboratory frame. Then perform a rotation-free boost from the laboratory frame to the $t\bar{t}$ center of momentum frame to define the $t$ ($\bar{t}$) direction in the $t\bar{t}$ center of momentum frame. Thirdly, boost the down-type fermion momenta, i.e., the lepton in leptonic top decays and the down-type quark in hadronic $W$ decays, from the $t\bar{t}$ center of momentum rotation-free to the $t$ and $\bar{t}$ rest frames. If the $t$ and $\bar{t}$ rest frames are constructed directly by boosting from the laboratory frame a Wigner rotation has to be taken into account [71].

Defining the angles $\theta_+$ and $\theta_-$ as described above, corresponds to studying spin correlations of the $t\bar{t}$ pair in the helicity basis.

It is important to stress that in spin correlation studies it is mandatory to reconstruct the top and the anti-top quark momenta. In the case of a double leptonic decay, two neutrino's are emitted and the full reconstruction of the event becomes non trivial. Imposing kinematic constraints, such as the known top and W masses, a constrained system of equations for the neutrino momenta can be set up. In general multiple solutions arise and the best solution can be only obtained on a statistical basis [21, 40, 73–77]. In the appendix some of the issues for the reconstruction are discussed in more detail. Alternatively, the single leptonic $t\bar{t}$ decay could be used by letting one of the jets of the hadronically decayed (anti-)top quark play the role of the lepton. Ideally, one would like to use the jet coming from the down-type quark, because it has the same (maximum) spin analyzing power as the lepton. In experiments one cannot easily distinguish between up- and down-type quarks
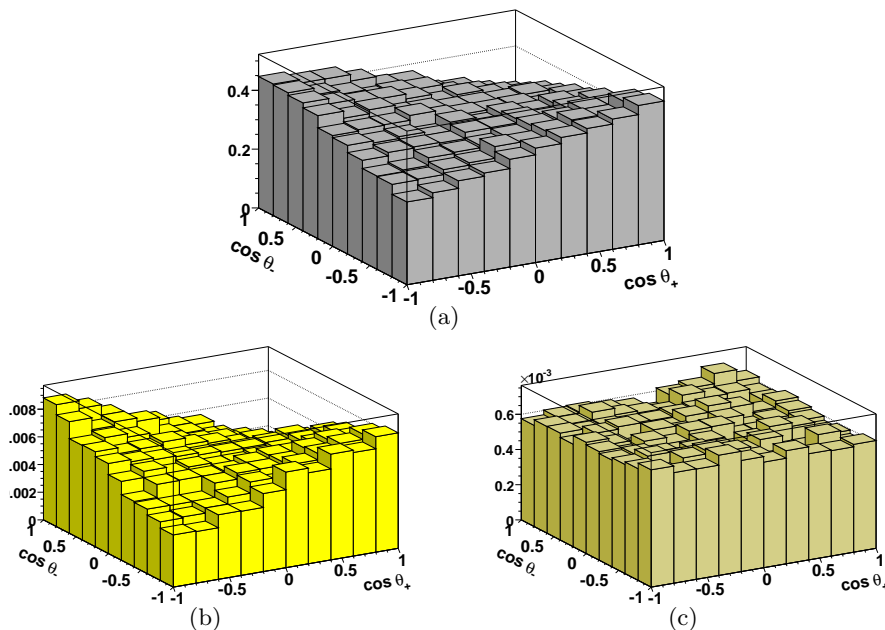
**Figure 16:** The distribution $\frac{1}{\sigma}\frac{d^2\sigma}{d\cos\theta_+ d\cos\theta_-}$ for SM $t\bar{t}$ production at the LHC, using pdf set CTEQ6L1, without applying cuts (a), and for the regions $390 < m_{t\bar{t}} < 410\,\mathrm{GeV}$ (b) and $790 < m_{t\bar{t}} < 810\,\mathrm{GeV}$ (c).

jets on event-by-event basis, and the analyzing power gets averaged $(1 - 0.3)/2 \approx 0.35$. However, improvements can be achieved by exploiting the fact that down-type quark jets have in general a smaller transverse momentum than the up-type quark jets. Using the least energetic (non-$b$) jet from the hadronic top decay increases the spin-analyzing power from 0.35 to approximately 0.5 [71, 72]. For illustrational purposes in the following we assume that the top quark momenta are correctly reconstructed and the spin analyzing power is maximal.

In figure 16 this distribution is plotted for QCD $t\bar{t}$ production.

The differences among the various $t\bar{t}$ production mechanisms are manifest. In figure 17 the distributions are plotted for resonance masses of $800\,\mathrm{GeV}$ for the following states:

- Scalar boson (a),

- Pseudo-scalar boson (b),

- Vector boson (c),

- Axial-vector boson (d),

- Vector-left boson (e),

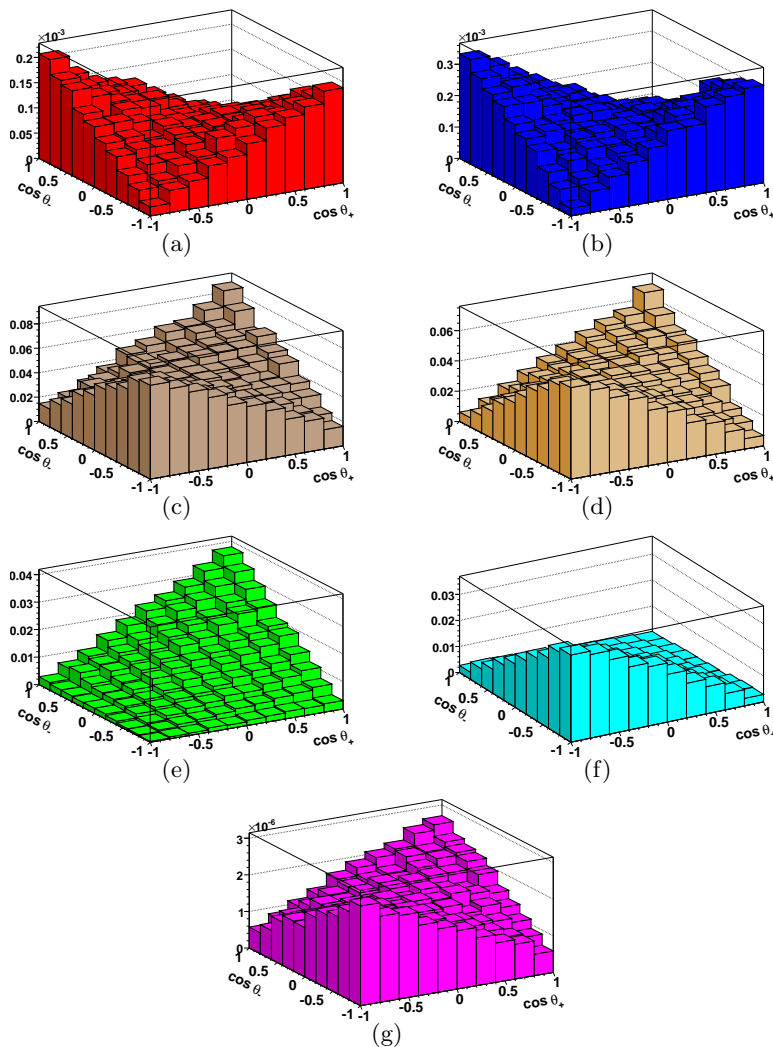- Vector-right boson (f),

- Spin-2 boson (g).

**Figure 17:** The distribution $\frac{1}{\sigma}\frac{d^2\sigma}{d\cos\theta_+ d\cos\theta_-}$ for (a) scalar, (b) pseudo-scalar, (c) vector, (d) axial-vector, (e) vector-left, (f) vector-right, (g) spin-2. $M_X = 800\,\text{GeV}$ at the LHC, using the pdf set CTEQ6L1. No cuts were applied.

With the vector-left and vector-right we understand a spin-1 vector boson that couples *only* to left- or right-handed fermions, respectively. We choose very narrow resonances by taking the width of resonances to be 1%, of the mass, i.e., $8\,\text{GeV}$ for a mass of $800\,\text{GeV}$. We do not include the SM QCD $t\bar{t}$ production background in these plots.

In table 2 the distributions are fitted to eq. (5.1) and compared with analytic computations. For the sake of simplicity, in the analytic computations the off-diagonal elements of the spin correlations matrix in the helicity basis are neglected. This means that the interference between different top quark spins are not included. In fact, the interference effects are negligible and the fitted values agree very well with the analytic computations. For completeness we also included the the numbers for a smaller resonance mass, $M_X = 400\,\text{GeV}$, where the effects from the mass of the top play a larger role.

The second angle, which is commonly considered when studying spin correlations in $t\bar{t}$

| resonance | mass (GeV) | $A$ calc. | $A$ fit. | $b_+$ calc. | $b_+$ fit. | $b_-$ calc. | $b_-$ fit. |
|---|---|---|---|---|---|---|---|
| sm | — | 0.319 | 0.304 | 0 | 0.008 | 0 | -0.003 |
| sm | $390 < m_{t\bar{t}} < 410$ | 0.501 | 0.532 | 0 | 0.004 | 0 | 0.005 |
| sm | $790 < m_{t\bar{t}} < 810$ | -0.061 | -0.051 | 0 | -0.014 | 0 | -0.011 |
| scalar | 400 | 1 | 0.972 | 0 | 0.005 | 0 | 0.007 |
| pseudo-scalar | 400 | 1 | 0.966 | 0 | 0.007 | 0 | 0.002 |
| vector | 400 | -0.449 | -0.432 | 0 | 0.008 | 0 | -0.004 |
| axial-vector | 400 | -1 | -0.990 | 0 | -0.004 | 0 | 0.002 |
| vector-left | 400 | -0.531 | -0.536 | 0.605 | 0.607 | 0.605 | 0.600 |
| vector-right | 400 | -0.531 | -0.558 | -0.605 | -0.604 | -0.605 | -0.610 |
| spin-2 | 400 | – | -0.348 | 0 | 0.001 | 0 | 0.006 |
| scalar | 800 | 1 | 0.985 | 0 | -0.015 | 0 | 0.004 |
| pseudo-scalar | 800 | 1 | 0.978 | 0 | -0.004 | 0 | -0.004 |
| vector | 800 | -0.826 | -0.819 | 0 | 0.008 | 0 | 0.005 |
| axial-vector | 800 | -1 | -1.001 | 0 | 0.008 | 0 | 0.008 |
| vector-left | 800 | -0.900 | -0.912 | 0.945 | 0.955 | 0.945 | 0.946 |
| vector-right | 800 | -0.900 | -0.884 | -0.945 | -0.938 | -0.945 | -0.943 |
| spin-2 | 800 | – | -0.743 | 0 | 0.022 | 0 | 0.013 |

**Table 2:** $\frac{1}{\sigma}\frac{d^2\sigma}{d\cos\theta_+ d\cos\theta_-} = \frac{1}{4}(1 - A\cos\theta_+\cos\theta_- + b_+\cos\theta_+ + b_-\cos\theta_-)$. For a top mass of 175 GeV. In the analytic calculation of the parameters, the interference between the various top spins is neglected.

production is $\phi$, i.e., the angle between the directions of the $f_d^+$ and $f_d^-$ in the $t$ and $\bar{t}$ rest frames, respectively. The distribution

$$\frac{1}{\sigma}\frac{d\sigma}{d\cos\phi} = \tfrac{1}{2}(1 - D\cos\phi), \tag{5.2}$$

for this angle is plotted in figure 18 for a resonance mass of 800 GeV.

The distributions for the angle $\phi$ are the same for production through a scalar and a vector boson. The distribution for the pseudo-scalar, on the other hand, is completely different from the one for the scalar and the vector boson [53]. Also, the angular distribution for SM $t\bar{t}$ production is different from the other production mechanisms. In the case of a spin-1 state, the $\phi$ distribution is independent of the type of coupling to the top: it makes no difference whether it is pure vector, an axial-vector, a left-handed or right-handed couplings.

## 6. Conclusions

Top physics is entering the precision phase at the Tevatron and will be one of the leading priorities at the LHC. The importance of the top quark in the quest for the mechanism of EWSB and new physics is due to the convergence of two factors. First the LHC will be a top factory with tens of millions of top quarks produced in the first years of running at the nominal low luminosity, $2 \times 10^{33}$ cm$^{-2}$ s$^{-1}$, allowing studies at an unprecedented level
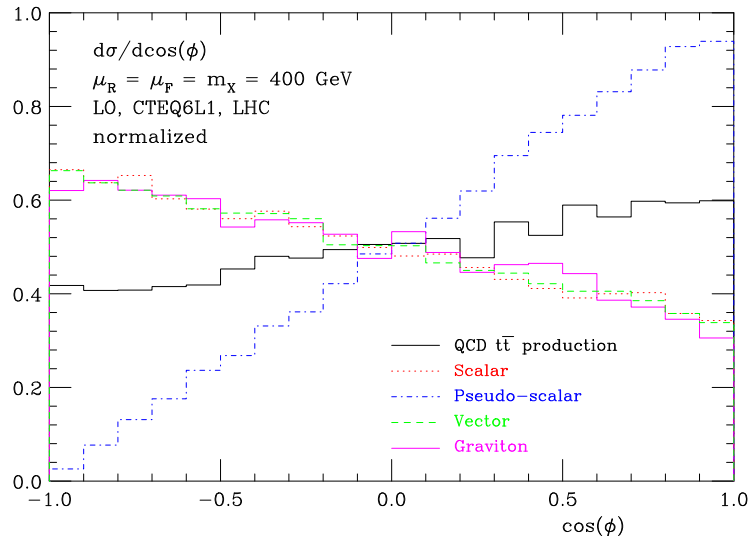
**Figure 18:** Distribution for the angle $\phi$, defined in the text, for different $t\bar{t}$ production mechanisms at the LHC. *Dark Solid* line is the SM $t\bar{t}$ production, *dotted line* is $t\bar{t}$ production through a scalar, *dot-dashed* line is $t\bar{t}$ production through a pseudo-scalar, *dashed* line is $t\bar{t}$ production through a vector (this is independent of the coupling). The *light solid* line is $t\bar{t}$ production through a graviton. The plots are normalized. The pdf set CTEQ6l1 is used with $M_X = 800\,\text{GeV}$ and $\mu_R = \mu_F = 800\,\text{GeV}$.

of accuracy. Second, due to its large mass, top is the optimal probe for new physics at TeV scales. Many different models, including the SM, predict the existence of heavy states that preferably couple to the top quark, and that could affect its SM couplings via loop corrections or be directly produced at the LHC.

Given the large number of the models proposed and their complexity, a "top-down" approach, e.g., model parameter scanning, will not be practical, in particular if comparison of many different channels and observables at once will be necessary. As an alternative, a simpler and more pragmatic "bottom-up" approach could be employed, whereby one identifies specific observables which can be developed as tools for discriminating generic features of new physics resonances, thus keeping the analysis as model independent as possible.

In this paper we have presented an example on how such a study could be performed for the invariant mass distribution of the $t\bar{t}$ pair.

As a first step we have assessed the accuracy of the best theoretical predictions available for $t\bar{t}$ production at hadron colliders. We have found that the shape of the distribution is under good theoretical control, especially at low invariant mass values, suggesting also the possibility of a precise top mass extraction.

We have then identified the features of new physics scenarios, namely the existence of heavy bosonic resonances of various spin, color and parity, that could show up in the $m_{t\bar{t}}$ distribution, and implemented them in the MadGraph/MadEvent package. The full matrix elements, $pp \to X \to t\bar{t} \to 6f$, $X$ being a spin-0, spin-1 or spin-2 particle, particles with arbitrary masses, width, color and couplings, have been automatically generated by MadGraph. The effects due to the interference with the $pp \to t\bar{t}$ SM process are included

when relevant.

The strategy to gain information on new physics is then straightforward and consists of three successive steps:

1. The discovery of the resonance (and the determination of its mass and width) which could appear as a sharp or broad peak or as a more distinctive peak-dip structure in very specific cases. In this measurement the key aspect will be the experimental resolution in the $m_{t\bar{t}}$ reconstruction.

2. The identification of the spin of the resonance, which can be inferred from the angular distribution of the top and the anti-top.

3. Information on the couplings of the resonance to the the top anti-top pair, which can be obtained by measuring the spin correlations of the top anti-top pair (for this last step the full matrix matrix element $2 \rightarrow 6$ is required).

In conclusion, we have outlined a simple strategy and provided the necessary Monte Carlo tools to search for new resonances in $t\bar{t}$ events. We look forward to more detailed experimental analyses.

## Acknowledgments

## A. Reconstruction issues in $t\bar{t}$ events

In this appendix we address some of the issues arising in the reconstruction of the $t\bar{t}$ events and in particular their different impact in the three-step analyses proposed above.

For a generic $2 \rightarrow 6$ process, where the final state particles masses are known, 16 independent variables are needed to determine the kinematics of the event: the six final state particle three-momenta, $\{\mathbf{p}_i\}$, the two energy fractions carried by the initial state partons, $x_{a,b}$, minus the overall momentum conservation which reduces the number of independent variables by 4, leads to $6 \times 3 + 2 - 4 = 16$.

From the measured angles and energies of the final state particles, together with constraints from $W$ boson and top quark masses, a system of equations can be set up to solve for the 16 unknown variables on an event-by-event basis.

The three decay modes of the $t\bar{t}$ pairs face each their own challenges for detection and reconstruction. Around 44% of the $t\bar{t}$ pairs decay hadronically, 30% of the $t\bar{t}$ pairs decay single-leptonically and 5% double leptonic (not including tau's) [40].[4] These three channels

---

[4]The remaining 21% are events including decays to tau's, which are not be considered here.

offer very different challenges related to the detection of final state particles and the reconstruction the (anti-)top quark momenta, which we will now address channel-by-channel.

The *fully-hadronic* decays have the advantage that in principle the momenta of all the final state particles can be determined, leading to $6 \times 3 = 18$ measurements. Together with the four mass constraints the system of equations for the 16 independent variables is over-constrained. Such constraints can be used in two ways. First they can be used to extract information, typically the jet energies, that have bad detector resolution. For example, measuring only the angles $(\theta, \phi)$ of the six jets and including all the constraints from the top quark and $W$ boson masses would already provide the required 16 independent quantities (althought with combinatorics). Alternatevely, the constraints from the masses can also be used to solve the combinatorics in reconstructing the $W$ boson and (anti-)top quark momenta. Combinatorics, affect each of the three steps in the analysis proposed in this paper in a different way. In the first step, i.e., the measurement of the $t\bar{t}$ invariant mass, section 3, combinatorics play no role: the invariant mass can be calculated by summing all the final state momenta irrespective of assigning jets to top or anti-top quarks, $W^+$ or $W^-$ bosons. In the second step, i.e. the measurement of the spin of an intermediate resonance, section 4, there is in principle a 12-fold ambiguity (assuming $b$-tagging) in assigning the correct ($b$-)jets to the top or anti-top quark. These ambiguities could be solved (in case of a very good jet energy resolution) or anyway allieviated by using the constraints from the top quark and $W$ masses. In the third step, i.e., the measurement of the spin correlations of the top anti-top pair, section 5, not all ambiguities can be solved: in any case is not possibly to uniquely identify on event-by-event basis which of the two jets come from the down-type quarks in the $W$ boson decays. Experimentally, the fully-hadronic decay is difficult to trigger and extract from multi-jet backgrounds, which makes this channel challgenging for BSM physics studies. [78]

The *single-lepton* decay channel is much more promising. The single lepton in the final state greatly improves the possibility for triggering on these events and extracting it from backgrounds compared to the fully-hadronic decay mode. The presence of a missing neutrino in the final state entails that only $5 \times 3 = 15$ independent measurements can be obtained, one short of 16 necessary. The missing information can be recovered by including a constraint coming from, e.g., the $W$ boson mass (up to a two-fold quadratic ambiguity, which can be solved in various ways, e.g., see ref. [34]). Using also the constraint from the top mass removes the ambiguity for assigning the correct $b$-jet to the top quark needed for second and third step in our analysis. For the third step, however, it is still non-trivial to solve the ambiguity coming from assigning the correct jet to the down-type quark in the non-leptonic $W$ decay. Several methods have been proposed, including, for example choosing the least energetic non-$b$-jet [71, 72]. Given its rate and the various reconstruction studies and possibilities, the single-lepton channel is the most straightforward search channel for BSM physics in $t\bar{t}$ events.

In the *double-lepton* decay mode there are two missing neutrino's in the final state. This makes the reconstruction of the full event kinematics challenging but certainly not impossible [21, 40, 73–77]. There are four visible particles in the final state, two $b$-jets and two opposite sign leptons, leading to $4 \times 3 = 12$ independent measurements. The

additional four constraints from the $W$ boson and top quark masses are just enough to set up a system of non-linear equations to solve for the necessary 16 variables. It can be shown that this system has up to eight solutions [74], of which, in general, only a few are physical and can be discarded or included based on their likelihood. It has to be noted that each solution has no further ambiguities and the event is completely reconstructed. For this reason, despite the small branching ratio, this channel competes in reach with the single-lepton in the studies of the spin correlation studies in $t\bar{t}$ [40, 79].

## References

[1] C.T. Hill, *Topcolor: top quark condensation in a gauge extension of the standard model*, *Phys. Lett.* **B 266** (1991) 419.

[2] C.T. Hill, *Topcolor assisted technicolor*, *Phys. Lett.* **B 345** (1995) 483 [`hep-ph/9411426`].

[3] C.T. Hill and S.J. Parke, *Top production: sensitivity to new physics*, *Phys. Rev.* **D 49** (1994) 4454 [`hep-ph/9312324`].

[4] R.M. Harris, C.T. Hill and S.J. Parke, *Cross section for topcolor Z'(t) decaying to $t\bar{t}$*, `hep-ph/9911288`.

[5] B.A. Dobrescu and C.T. Hill, *Electroweak symmetry breaking via top condensation seesaw*, *Phys. Rev. Lett.* **81** (1998) 2634 [`hep-ph/9712319`].

[6] R.S. Chivukula, B.A. Dobrescu, H. Georgi and C.T. Hill, *Top quark seesaw theory of electroweak symmetry breaking*, *Phys. Rev.* **D 59** (1999) 075003 [`hep-ph/9809470`].

[7] H.-J. He, C.T. Hill and T.M.P. Tait, *Top quark seesaw, vacuum structure and electroweak precision constraints*, *Phys. Rev.* **D 65** (2002) 055006 [`hep-ph/0108041`].

[8] C.T. Hill and E.H. Simmons, *Strong dynamics and electroweak symmetry breaking*, *Phys. Rept.* **381** (2003) 235 [*Erratum ibid.* **390** (2004) 553] [`hep-ph/0203079`].

[9] N. Arkani-Hamed, A.G. Cohen and H. Georgi, *Electroweak symmetry breaking from dimensional deconstruction*, *Phys. Lett.* **B 513** (2001) 232 [`hep-ph/0105239`].

[10] N. Arkani-Hamed, A.G. Cohen, T. Gregoire and J.G. Wacker, *Phenomenology of electroweak symmetry breaking from theory space*, *JHEP* **08** (2002) 020 [`hep-ph/0202089`].

[11] N. Arkani-Hamed et al., *The minimal moose for a little Higgs*, *JHEP* **08** (2002) 021 [`hep-ph/0206020`].

[12] N. Arkani-Hamed, A.G. Cohen, E. Katz and A.E. Nelson, *The littlest Higgs*, *JHEP* **07** (2002) 034 [`hep-ph/0206021`].

[13] I. Low, W. Skiba and D. Tucker-Smith, *Little Higgses from an antisymmetric condensate*, *Phys. Rev.* **D 66** (2002) 072001 [`hep-ph/0207243`].

[14] T. Han, H.E. Logan, B. McElrath and L.-T. Wang, *Phenomenology of the little Higgs model*, *Phys. Rev.* **D 67** (2003) 095004 [`hep-ph/0301040`].

[15] G. Azuelos et al., *Exploring little Higgs models with ATLAS at the LHC*, *Eur. Phys. J.* **C 39S2** (2005) 13 [`hep-ph/0402037`].

[16] M. Schmaltz and D. Tucker-Smith, *Little Higgs review*, *Ann. Rev. Nucl. Part. Sci.* **55** (2005) 229 [`hep-ph/0502182`].

[17] N. Arkani-Hamed, S. Dimopoulos and G.R. Dvali, *The hierarchy problem and new dimensions at a millimeter*, *Phys. Lett.* **B 429** (1998) 263 [hep-ph/9803315].

[18] L. Randall and R. Sundrum, *A large mass hierarchy from a small extra dimension*, *Phys. Rev. Lett.* **83** (1999) 3370 [hep-ph/9905221].

[19] A.L. Fitzpatrick, J. Kaplan, L. Randall and L.-T. Wang, *Searching for the Kaluza-Klein graviton in bulk RS models*, *JHEP* **09** (2007) 013 [hep-ph/0701150].

[20] M. Arai, N. Okada, K. Smolek and V. Simak, *Top spin correlations in theories with large extra-dimensions at the Large Hadron Collider*, *Phys. Rev.* **D 70** (2004) 115015 [hep-ph/0409273].

[21] M. Arai, N. Okada, K. Smolek and V. Simak, *Top quark spin correlations in the Randall-Sundrum model at the CERN Large Hadron Collider*, *Phys. Rev.* **D 75** (2007) 095008 [hep-ph/0701155].

[22] C.D. McMullen and S. Nandi, *Collider implications of Kaluza-Klein excitations of the electroweak gauge bosons*, hep-ph/0110275.

[23] K. Agashe, A. Delgado, M.J. May and R. Sundrum, *RS1, custodial isospin and precision tests*, *JHEP* **08** (2003) 050 [hep-ph/0308036].

[24] K. Agashe, A. Belyaev, T. Krupovnickas, G. Perez and J. Virzi, *LHC signals from warped extra dimensions*, *Phys. Rev.* **D 77** (2008) 015003 [hep-ph/0612015].

[25] B. Lillie, L. Randall and L.-T. Wang, *The bulk RS KK-gluon at the LHC*, *JHEP* **09** (2007) 074 [hep-ph/0701166].

[26] A. Djouadi, G. Moreau and R.K. Singh, *Kaluza-Klein excitations of gauge bosons at the LHC*, *Nucl. Phys.* **B 797** (2008) 1 [arXiv:0706.4191].

[27] R. Ghavri, C.D. McMullen and S. Nandi, *Collider implications of multiple non-universal extra dimensions*, *Phys. Rev.* **D 74** (2006) 015012 [hep-ph/0602014].

[28] G. Burdman, B.A. Dobrescu and E. Ponton, *Resonances from two universal extra dimensions*, *Phys. Rev.* **D 74** (2006) 075008 [hep-ph/0601186].

[29] B. Lillie, J. Shu and T.M.P. Tait, *Kaluza-Klein gluons as a diagnostic of warped models*, *Phys. Rev.* **D 76** (2007) 115016 [arXiv:0706.3960].

[30] K. Agashe et al., *LHC signals for warped electroweak neutral gauge bosons*, *Phys. Rev.* **D 76** (2007) 115015 [arXiv:0709.0007].

[31] T. Stelzer and W.F. Long, *Automatic generation of tree level helicity amplitudes*, *Comput. Phys. Commun.* **81** (1994) 357 [hep-ph/9401258].

[32] F. Maltoni and T. Stelzer, *MadEvent: automatic event generation with MadGraph*, *JHEP* **02** (2003) 027 [hep-ph/0208156].

[33] J. Alwall et al., *MadGraph/MadEvent v4: the new web generation*, *JHEP* **09** (2007) 028 [arXiv:0706.2334].

[34] V. Barger, T. Han and D.G.E. Walker, *Top quark pairs at high invariant mass — a model-independent discriminator of new physics at the LHC*, *Phys. Rev. Lett.* **100** (2008) 031801 [hep-ph/0612016].

[35] U. Baur and L.H. Orr, *High $p_T$ top quarks at the Large Hadron Collider*, *Phys. Rev.* **D 76** (2007) 094012 [arXiv:0707.2066].

[36] M. Cacciari, S. Frixione, M.L. Mangano, P. Nason and G. Ridolfi, *The $t\bar{t}$ cross-section at 1.8 TeV and 1.96 TeV: a study of the systematics due to parton densities and scale dependence*, *JHEP* **04** (2004) 068 [hep-ph/0303085].

[37] J.M. Campbell and R.K. Ellis, *An update on vector boson pair production at hadron colliders*, *Phys. Rev.* **D 60** (1999) 113006 [hep-ph/9905386].

[38] J. Pumplin et al., *New generation of parton distributions with uncertainties from global QCD analysis*, *JHEP* **07** (2002) 012 [hep-ph/0201195].

[39] R. Bonciani, S. Catani, M.L. Mangano and P. Nason, *NLL resummation of the heavy-quark hadroproduction cross-section*, *Nucl. Phys.* **B 529** (1998) 424 [*Erratum ibid.* **B 803** (2008) 234] [hep-ph/9801375].

[40] M. Beneke et al., *Top quark physics*, hep-ph/0003033.

[41] M. Cacciari, private communication.

[42] S. Frixione, P. Nason and B.R. Webber, *Matching NLO QCD and parton showers in heavy flavour production*, *JHEP* **08** (2003) 007 [hep-ph/0305252].

[43] J.H. Kuhn, A. Scharf and P. Uwer, *Electroweak effects in top-quark pair production at hadron colliders*, *Eur. Phys. J.* **C 51** (2007) 37 [hep-ph/0610335].

[44] W. Bernreuther, M. Fuecker and Z.-G. Si, *Weak interaction corrections to hadronic top quark pair production*, *Phys. Rev.* **D 74** (2006) 113005 [hep-ph/0610334].

[45] P. Ferrari, *Early physics with top quarks at the LHC*, arXiv:0705.3021.

[46] U. Baur and L.H. Orr, *Searching for $t\bar{t}$ resonances at the Large Hadron Collider*, *Phys. Rev.* **D 77** (2008) 114001 [arXiv:0803.1160].

[47] S. Moch and P. Uwer, *Theoretical status and prospects for top-quark pair production at hadron colliders*, *Phys. Rev.* **D 78** (2008) 034003 [arXiv:0804.1476].

[48] M.C. Smith and S.S. Willenbrock, *Top-quark pole mass*, *Phys. Rev. Lett.* **79** (1997) 3825 [hep-ph/9612329].

[49] T. Sjöstrand, S. Mrenna and P. Skands, *PYTHIA 6.4 physics and manual*, *JHEP* **05** (2006) 026 [hep-ph/0603175].

[50] G. Corcella et al., *HERWIG 6.4 release note*, hep-ph/0201201.

[51] K.J.F. Gaemers and F. Hoogeveen, *Higgs production and decay into heavy flavors with the gluon fusion mechanism*, *Phys. Lett.* **B 146** (1984) 347.

[52] D. Dicus, A. Stange and S. Willenbrock, *Higgs decay to top quarks at hadron colliders*, *Phys. Lett.* **B 333** (1994) 126 [hep-ph/9404359].

[53] W. Bernreuther, M. Flesch and P. Haberl, *Signatures of Higgs bosons in the top quark decay channel at hadron colliders*, *Phys. Rev.* **D 58** (1998) 114031 [hep-ph/9709284].

[54] A.V. Manohar and M.B. Wise, *Flavor changing neutral currents, an extended scalar sector and the Higgs production rate at the LHC*, *Phys. Rev.* **D 74** (2006) 035009 [hep-ph/0606172].

[55] M.I. Gresham and M.B. Wise, *Color octet scalar production at the LHC*, *Phys. Rev.* **D 76** (2007) 075003 [arXiv:0706.0909].

[56] E.H. Simmons, *Coloron phenomenology*, *Phys. Rev.* **D 55** (1997) 1678 [hep-ph/9608269].

[57] D. Choudhury, R.M. Godbole, R.K. Singh and K. Wagh, *Top production at the Tevatron/LHC and nonstandard, strongly interacting spin one particles*, *Phys. Lett.* **B 657** (2007) 69 [arXiv:0705.1499].

[58] D.A. Dicus, C.D. McMullen and S. Nandi, *Collider implications of Kaluza-Klein excitations of the gluons*, *Phys. Rev.* **D 65** (2002) 076007 [hep-ph/0012259].

[59] A. Djouadi, *The anatomy of electro-weak symmetry breaking. II: the Higgs bosons in the minimal supersymmetric model*, *Phys. Rept.* **459** (2008) 1 [hep-ph/0503173].

[60] K. Cheung and W.-Y. Keung, *Split supersymmetry, stable gluino and gluinonium*, *Phys. Rev.* **D 71** (2005) 015015 [hep-ph/0408335].

[61] P.H. Frampton and S.L. Glashow, *Unifiable chiral color with natural GIM mechanism*, *Phys. Rev. Lett.* **58** (1987) 2168.

[62] P.H. Frampton and S.L. Glashow, *Chiral color: an alternative to the Standard Model*, *Phys. Lett.* **B 190** (1987) 157.

[63] O. Antunano, J.H. Kuhn and G. Rodrigo, *Top quarks, axigluons and charge asymmetries at hadron colliders*, *Phys. Rev.* **D 77** (2008) 014003 [arXiv:0709.1652].

[64] N. Arkani-Hamed, S. Dimopoulos and G.R. Dvali, *Phenomenology, astrophysics and cosmology of theories with sub-millimeter dimensions and TeV scale quantum gravity*, *Phys. Rev.* **D 59** (1999) 086004 [hep-ph/9807344].

[65] L. Randall and R. Sundrum, *An alternative to compactification*, *Phys. Rev. Lett.* **83** (1999) 4690 [hep-th/9906064].

[66] J.C. Collins and D.E. Soper, *Angular distribution of dileptons in high-energy hadron collisions*, *Phys. Rev.* **D 16** (1977) 2219.

[67] J. Alwall et al., *Is $V_{tb} \simeq 1$?*, *Eur. Phys. J.* **C 49** (2007) 791 [hep-ph/0607115].

[68] S. Willenbrock, *The standard model and the top quark*, hep-ph/0211067.

[69] M. Jezabek and J.H. Kuhn, *V-A tests through leptons from polarized top quarks*, *Phys. Lett.* **B 329** (1994) 317 [hep-ph/9403366].

[70] A. Czarnecki, M. Jezabek and J.H. Kuhn, *Lepton spectra from decays of polarized top quarks*, *Nucl. Phys.* **B 351** (1991) 70.

[71] W. Bernreuther, A. Brandenburg, Z.G. Si and P. Uwer, *Top quark pair production and decay at hadron colliders*, *Nucl. Phys.* **B 690** (2004) 81 [hep-ph/0403035].

[72] G. Mahlon and S.J. Parke, *Angular correlations in top quark pair production and decay at hadron colliders*, *Phys. Rev.* **D 53** (1996) 4886 [hep-ph/9512264].

[73] R.H. Dalitz and G.R. Goldstein, *Analysis of top-antitop production and dilepton decay events and the top quark mass*, *Phys. Lett.* **B 287** (1992) 225.

[74] L. Sonnenschein, *Analytical solution of $t\bar{t}$ dilepton equations*, *Phys. Rev.* **D 73** (2006) 054015 [*Erratum ibid.* **D 78** (2008) 079902] [hep-ph/0603011].

[75] CDF collaboration, D.E. Acosta et al., *Search for anomalous kinematics in $t\bar{t}$ dilepton events at CDF II*, *Phys. Rev. Lett.* **95** (2005) 022001 [hep-ex/0412042].

[76] M. Baarmand et al., *Measurement of spin correlation in top quark pair production in semi-leptonic final state*, CERN-CMS-NOTE-2006-111 (2006).

[77] K. Smolek and V. Simák, *Measurement of spin correlations of top-antitop pairs*, ATL-PHYS-2003-012 (2003).

[78] CMS collaboration, G.L. Bayatian et al., *CMS technical design report, volume II: physics performance*, *J. Phys.* **G 34** (2007) 995.

[79] I. Borjanovic et al., *Investigation of top mass measurements with the ATLAS detector at LHC*, *Eur. Phys. J.* **C 39S2** (2005) 63 [hep-ex/0403021].